# Full-field measurement of lightweight nonlinear structures using 3D SLDV

Xing Wang,*

School of Aeronautics and Astronautics, Shenzhen Campus of Sun Yat-sen University, Shenzhen 518107, People's Republic of China. Shenzhen Key Laboratory of Intelligent Microsatellite Constellation, Shenzhen 518107, People's Republic of China.

Jie Yuan,†

Computational Engineering Design Group, University of Southampton, Southampton SO17 1BJ, United Kingdom.

Michal Szydlowski,‡ and Christoph Schwingshackl §

Department of Mechanical Engineering, Imperial College London, London SW7 2AZ, United Kingdom.

## Abstract

Modern non-contact measurement techniques such as the Three-dimensional Scanning Laser Doppler Vibrometry (3D SLDV) are advantageous in measuring vibrations of lightweight, thin-walled aerospace structures, which were conventionally deemed as difficult or not feasible to apply using attached transducers. Nevertheless, the full-field measurements using 3D SLDV are still limited to extracting modal properties of linear structures, while measurements of complex nonlinear structures are rarely reported. This paper aims to extend the full-field measurement capability of

*Associate Professor, School of Aeronautics and Astronautics, Shenzhen Campus of Sun Yat-sen University; also Shenzhen Key Laboratory of Intelligent Microsatellite Constellation; Shenzhen 518107, People's Republic of China; wangxing5@mail.sysu.edu.cn. (Corresponding Author)

†Lecturer, Computational Engineering Design Group, University of Southampton, Southampton SO17 1BJ, United Kingdom.

‡Postdoc, Department of Mechanical Engineering, Imperial College London , London SW7 2AZ, United Kingdom.

§Reader, Department of Mechanical Engineering, Imperial College London, London SW7 2AZ, United Kingdom.

3D SLDV and combines it with a Multiple-Input-Single-Output (MISO) vibration controller to deal with nonlinear structures. An advanced test strategy is introduced, which is capable of obtaining amplitude-dependent resonant frequencies, modal damping ratios and full-field, multi-harmonic mode shapes of nonlinear normal modes (NNMs). Conflicting parameters such as the frequency resolution and measurement time are optimised by combining phase separation and phase resonance testing techniques in a coherent strategy. The capabilities of the proposed nonlinear modal testing strategy are demonstrated on a realistic, large-scale fan blade that exhibits softening behaviours. Two of its NNMs were investigated at larger vibration amplitudes. Its nonlinear modal parameters were successfully extracted and validated, highlighting the time efficiency and data accuracy of the proposed strategy for measuring industrial-scale, lightweight nonlinear structures.

**Keywords:** 3D SLDV, advanced test strategy, full-field measurement, lightweight nonlinear structures.

## I. Introduction

The drive towards more optimised design for improved fuel efficiency and reduced carbon emissions has led to even thinner, slender and lighter aerospace structure designs. These newly developed structures are expected to undergo harsher loads and experience much larger deformations, resulting in stronger nonlinear vibrations. In this regard, conventional linear modal testing techniques and measurement equipment need to be extended to accommodate these nonlinearities, such as identifying amplitude-dependent modal properties or measuring multi-harmonic responses.

Many researchers attempt to combine the nonlinear modal testing techniques and the contact transducers such as accelerometers or strain gauges in vibration testing of nonlinear structures. One type of such test is to resort to phase separation testing techniques, which involve measuring nonlinear Frequency Responses (FRs) or Frequency Response Functions (FRFs) using stepped-sine or slowly swept-sine excitations at multiple input levels. Then, the nonlinear modal frequency and damping ratio could be simultaneously identified by curve-fitting a nonlinear modal model to the frequency response curves [1,2]. In the test, constant input force is routinely required when measuring such curves. Recently, it has been relaxed in Refs [3,4]. From another perspective, the response of the nonlinear structural responses could be controlled in the test such that the dynamics would be linearised at the response level; this leads to the response-controlled stepped-sine testing (RCT) technique, which has been successfully applied to a nonlinear structure with a single grounded nonlinear element [5] or an industrial structure such as a missile [6]. Additionally, other techniques, such as the fixed frequency voltage control (FFVC) tests [7], also demonstrated advantages in obtaining multivalued phase curves. The second type of vibration test for nonlinear structures is called the *normal-mode force appropriation* [8] (also known as the phase resonance testing technique). Peeters *et al*. [9,10] were the first to apply the phase resonance testing technique to a nonlinear structure experimentally, in which the frequency of a sinusoidal input force was manually adjusted to meet the *local phase-lag quadrature criterion*. In the test, the phase lag between the input force and the displacement response at the excitation point was tuned to 90°, and the structure was then believed to vibrate according to a single NNM [10]. Subsequently, the phase-lag adjustment process was automated using Phase-Locked-Loop (PLL) controllers [11,12,13], Control-Based Continuation (CBC) methods [14,15,16,17], or resonance tracking controllers [18,19]. Recently, the PLL and CBC methods were also compared on the same benchmark system in Ref [20], and the excellent agreement of the measured backbone and frequency response curves proved the feasibility of the two testing methods.

In addition to the abovementioned contact measurement techniques, there is a strong demand to apply non-contact measurement techniques to the vibration testing of nonlinear structures. This is particularly important for lightweight or thin-walled structures that are sensitive to the mass-loading effects of attached transducers. The vibration testing techniques in these applications are often developed with individual non-contact measurement equipment. For video-based measurement equipment, nonlinear testing techniques such as free decay or forced vibration can be applied directly. High-speed videos and advanced image processing algorithms are used to estimate structural vibrations by performing edge detection [21] or Digital Image Correlation (DIC) [22]. The test structure has to be seen by all the cameras, leading to size limitations and requirements of dedicated surface preparation. The displacement measurement resolution and sampling frequency range of these video-based measurement techniques are also concerns for industrial applications. Laser-based measurement equipment generally provides better resolutions and a wider bandwidth of sampling capabilities [23]. Because most laser measurement equipment is indeed a single transducer, the synchronisation of measurement data and time efficiency are vital challenges when measuring nonlinear structural vibrations. Many researchers used it to measure nonlinear FRFs of a single point [24,25] and showed that it is sufficient to identify nonlinear resonant frequency and damping ratios of a complex structure. When spatially detailed vibration patterns are of interest, Continuous Scanning Laser Doppler Vibrometry (CSLDV) [26] was first introduced. Ehrhardt *et al*. [27,28] presented initial works on the full-field measurements of nonlinear structures using a Three-dimensional DIC system and a CSLDV. It was shown that up to 6 harmonics of the deformation shapes of a nonlinear beam or plate could be extracted; the higher-order harmonics were found to be smaller than the measurement resolution, hindering the application of this technique to estimate high-frequency vibrations of test structures. The three-dimensional Scanning Laser Doppler Vibrometry (3D SLDV) is another laser-based equipment that has been considered in the full-field measurement of aerospace structures of various sizes, frequency ranges, and geometrical complexities [29]. Its full-field measurement applications were previously limited to linear structures. Recently, the authors of this paper removed this limitation by developing a multi-step Interpolated-FFT procedure [19] to estimate multiple harmonics from super-short sampling intervals. However, such a measurement procedure needs to be integrated into a vibration test strategy in order to identify the nonlinear modal properties accurately and efficiently.

This paper proposes a test setup for the full-field measurement of nonlinear modal parameters using 3D SLDV. The setup combines the 3D SLDV with a Multiple Input Single Output (MISO) vibration controller, where the former performs non-contact, full-field measurements, and the latter applies dedicated input forces. Based on the test setup, a full-field nonlinear modal testing strategy consisting of three phases is proposed to quantify the nonlinear modal parameters of the test structure. In Phase I, conventional full-field linear modal testing is conducted using low-amplitude excitations to measure the natural frequencies, damping ratios and full-field mode shapes of the underlying linear system. Phase II then detects the NNMs of the structure and applies a fast nonlinear phase resonance test to track the backbone curve of each NNM; the amplitude-dependent modal frequencies and damping ratios are then extracted from the test data. A sine-dwell test is subsequently performed along the backbone curve, and the full-field, multi-harmonic mode shapes are estimated using measured datasets of 3D SLDV. A validation step for the extracted nonlinear modal parameters is carried out at the end of Phase II. Finally, in Phase III, the integrity of the test structure is checked to ensure that no recognisable damage occurs during the testing campaign. The proposed strategy is applied to an aero-engine fan blade with complex three-dimensional curvature, demonstrating that it allows for time-efficient and accurate extraction of full-field modal parameters with fine frequency and spatial resolutions that meet stringent industry standards.

The following paper is organised as follows: Sec. Ⅱ details the theoretical background of nonlinear modal testing. Sec. Ⅲ elaborates on the test setup and the proposed test strategy. Sec. Ⅳ illustrates the proposed strategy using an industrial-scale fan blade, and Sec. Ⅴ draws conclusions.

## II. Theoretical background

This paper considers the dynamics of a general structure with both stiffness and damping nonlinearities. After spatial discretisation into an *N*-degree-of-freedom (*N*-DOF) system, its forced dynamic equation of motion can be written as:

$$\mathbf{M}\ddot{\boldsymbol{u}} + \mathbf{C}\dot{\boldsymbol{u}} + \mathbf{K}\boldsymbol{u} + \boldsymbol{f}_{\mathrm{nl}}\left(\boldsymbol{u}, \dot{\boldsymbol{u}}\right) = \boldsymbol{p}\left(t\right), \tag{1}$$

where $\mathbf{M} \in \mathbb{R}^{N\times N}$, $\mathbf{C} \in \mathbb{R}^{N\times N}$, $\mathbf{K} \in \mathbb{R}^{N\times N}$ denote the mass, damping and stiffness matrices, respectively. Vectors $\ddot{\boldsymbol{u}} \in \mathbb{R}^{N\times 1}$, $\dot{\boldsymbol{u}} \in \mathbb{R}^{N\times 1}$ and $\boldsymbol{u} \in \mathbb{R}^{N\times 1}$ represent the acceleration, velocity and displacement, respectively. $\boldsymbol{p}\left(t\right) \in \mathbb{R}^{N\times 1}$ is the external excitation force vector applied to the test structure while $\boldsymbol{f}_{\mathrm{nl}}\left(\boldsymbol{u}, \dot{\boldsymbol{u}}\right) \in \mathbb{R}^{N\times 1}$ represents the internal nonlinear force vector.

The proposed testing strategy is based on the concept of NNM and mode isolation testing techniques. A brief overview of these techniques is provided, and derivations of the amplitude-dependent modal frequencies, modal damping ratios, and mode shapes from the perspective of experimental modal analysis are presented.

### A. Nonlinear Normal Mode

In analogous to *real normal mode* analysis of linear systems, the nonlinear modes of the associated undamped system are sought first. To allow the computation of real nonlinear modes of a system, it is assumed that the nonlinear force vector in Eq. (1) can be decoupled in the form of:

$$\boldsymbol{f}_{\mathrm{nl}}(\boldsymbol{u},\dot{\boldsymbol{u}})=\boldsymbol{f}_{\mathrm{nl}}^{\mathrm{u}}(\boldsymbol{u})+\boldsymbol{f}_{\mathrm{nl}}^{\mathrm{d}}(\dot{\boldsymbol{u}}), \tag{2}$$

where $\boldsymbol{f}_{\mathrm{nl}}^{\mathrm{u}}(\boldsymbol{u})$ and $\boldsymbol{f}_{\mathrm{nl}}^{\mathrm{d}}(\dot{\boldsymbol{u}})$ represent the conservative and dissipative internal nonlinear forces, respectively.

In this work, the definition of NNM proposed by Kerschen *et al.* [30] is used, where a NNM is defined as periodic motion governed by the conservative, autonomous part of Eq. (1), i.e.,

$$\mathbf{M}\ddot{\boldsymbol{u}}+\mathbf{K}\boldsymbol{u}+\boldsymbol{f}_{\mathrm{nl}}^{\mathrm{u}}(\boldsymbol{u})=\mathbf{0}. \tag{3}$$

To compute the NNMs of Eq. (3), non-trivial solutions approximated by truncated Fourier series [30,31] are used:

$$\boldsymbol{u}(t)=\mathrm{Re}\left(\sum_{n=0}^{N_h}\tilde{\boldsymbol{\psi}}^{(n)}e^{\mathrm{j}n\tilde{\omega}t}\right), \tag{4}$$

where $\tilde{\boldsymbol{\psi}}^{(n)}$ denotes the real-valued, $n$-th harmonic mode shape, $\tilde{\omega}$ is the nonlinear modal frequency, $N_h$ denotes the maximum order of truncated harmonics, and $\mathrm{j}=\sqrt{-1}$ denotes the imaginary unit. The notion $\tilde{\bullet}$ indicates that the parameter is dependent on the vibration amplitude. The periodic motion definition of NNM implies that its mode shape contains multiple harmonics, as represented by $\tilde{\boldsymbol{\psi}}^{(0)}$, $\tilde{\boldsymbol{\psi}}^{(1)}$, …$\tilde{\boldsymbol{\psi}}^{(N_h)}$.

Inserting the truncated Fourier bases - Eq. (4) - into Eq. (3) and removing the time dependency with a Galerkin projection, one gets a set of algebraic equations:

$$\mathbf{Z}^{(n)}(\tilde{\omega})\tilde{\boldsymbol{\psi}}_n+\boldsymbol{F}_{\mathrm{nl}}^{\mathrm{u}(n)}(\tilde{\boldsymbol{U}})=\mathbf{0},\quad n=0,1,\cdots N_h. \tag{5}$$

where $\mathbf{Z}^{(n)}(\tilde{\omega})=-(n\tilde{\omega})^2\mathbf{M}+\mathbf{K}$ are blocks of the dynamic stiffness matrix, $\tilde{\boldsymbol{U}}=\left[\tilde{\boldsymbol{\psi}}^{(0)},\tilde{\boldsymbol{\psi}}^{(1)},\cdots\tilde{\boldsymbol{\psi}}^{(N_h)}\right]$ contains multi-harmonic mode shapes, and $\boldsymbol{F}_{\mathrm{nl}}^{\mathrm{u}(n)}$ represents the complex amplitude of the multi-harmonic internal nonlinear forces. In the computation of NNMs, Eq. (5) is solved via a continuation algorithm [30,32], while in this paper, the NNM parameters will be directly estimated from test data.

## B. Single-NNM Motion

It is supposed that the test structure is lightly damped and, in the test, each NNM is excited sequentially by a dedicated external force (usually a single sinusoidal force), i.e.

$$\boldsymbol{p}(t)=\mathrm{Re}\left(\boldsymbol{p}e^{\mathrm{j}\Omega t}\right). \tag{6}$$

where $\Omega$ is the driving frequency of the external force, and vector $\boldsymbol{p}$ represents the force amplitude.

It is subsequently assumed that the NNM is well-isolated; therefore, the single-NNM method can be applied to the forced and damped dynamic equation - Eq. (1) - to reduce its dimension. Many variants of single NNM methods have been proposed, such as the NNM motion which contains a primary harmonic term only [33] or multi-harmonic terms [34]. This paper follows the latter assumption such that, using the near-resonant condition $\Omega \approx \tilde{\omega}_r$, the structural responses are dominated by a single nonlinear mode with many harmonics:

$$\boldsymbol{u}(t) \approx \boldsymbol{u}_r(t)=\mathrm{Re}\left(\sum_{n=0}^{N_h}\tilde{\boldsymbol{U}}_r^{(n)}e^{\mathrm{j}n\Omega t}\right)=\mathrm{Re}\left(\sum_{n=0}^{N_h}\tilde{\boldsymbol{\phi}}_r^{(n)}q_r e^{\mathrm{j}n\Omega t}\right), \tag{7}$$

where $\tilde{\boldsymbol{U}}_r^{(n)}$ denotes the amplitude of the forced responses of the $r$th mode.

In Eq. (7), the deflection shape $\tilde{\boldsymbol{U}}_r^{(n)}$ is linked to the normalised mode shape via the modal amplitude:

$$\tilde{\boldsymbol{U}}_r^{(n)}=\tilde{\boldsymbol{\phi}}_r^{(n)}q_r, \tag{8}$$

where $q_r$ denotes the complex-valued amplitude of the $r$-th resonant NNM. $\tilde{\boldsymbol{\phi}}_r$ represents the amplitude-dependent, normalised nonlinear mode shape scaled from $\boldsymbol{\psi}_r$, which is a real-valued vector. Note that several normalisation approaches have been proposed for nonlinear mode shapes, of which the mass normalisation of the fundamental harmonic shape [34] is often used in numerical analysis. However, using deflection shape ($\tilde{\boldsymbol{U}}_r^{(n)}$) is preferred in experimental modal analysis since it involves much less manipulation of test data.

One advantage of the single-NNM method is that it allows reducing the forced and damped equation - Eq. (1) - onto each NNM coordinate by means of the Ritz-Galerkin procedure [34,35], leading to a series of single-NNM dynamic equations:

$$\left(\left(\tilde{\omega}_r^2-\Omega^2\right)\tilde{m}_r+\mathrm{j}\tilde{c}_r\Omega\right)q_r=\left(\tilde{\boldsymbol{\phi}}_r^{(1)}\right)^{\mathrm{T}}\boldsymbol{p}, \tag{9}$$

$$\left(\left(\tilde{\omega}_r^2-n^2\Omega^2\right)\tilde{m}_r+\mathrm{j}n\tilde{c}_r\Omega\right)q_r=0, \quad n=2\cdots N_h, \tag{10}$$

where $\tilde{m}_r$ and $\tilde{c}_r$ denote the modal mass and modal viscous damping coefficient, respectively. The modal mass, damping ratio and modal frequency for the $r$-th NNM are denoted using $\tilde{\bullet}$ to indicate the amplitude dependency. Since deriving an accurate damping model for a realistic structure is extremely difficult, this paper uses a nonlinear viscous modal damping coefficient ($\tilde{c}_r$) in Eq. (9) to account for the energy dissipation. In fact, the modal viscous damping model is only valid when the coupling damping terms between NNMs are negligible [9-17]. Fortunately, this assumption has proven to be quite accurate and useful for a wide range of realistic structures [9-17].

A comprehensive derivation of the single-NNM reduction process can be found in Ref [34]. Herein, this paper uses the single-NNM equation inversely to identify nonlinear modal parameters through experimental test data.

## C. Experimental Mode Isolation

The experimental technique to achieve single-mode isolation is often referred to as *normal-mode force appropriation* (or phase resonance testing) [9,36], in which the so-called *local phase quadrature criterion* is widely adopted for lightly-damped structures [12]. This technique is also used in the proposed test strategy and is briefly revisited.

Ideally, a NNM is appropriated when the external force cancels all the internal damping of the test structure [9-13, 27], i.e.

$$\mathbf{C}\dot{\boldsymbol{u}} + \boldsymbol{f}_{\mathrm{nl}}^{\mathrm{d}}(\dot{\boldsymbol{u}}) = \boldsymbol{p}(t), \forall t. \tag{11}$$

Eq.(11) represents a condition of *perfect force appropriation* [12], which is not practically feasible due to multiple reasons [9-13, 27]: i) the viscous damping model of the test structure is simply an assumption. In practice, the damping matrix $\mathbf{C} \in \mathbb{R}^{N\times N}$ and the internal nonlinear damping force $\boldsymbol{f}_{\mathrm{nl}}^{\mathrm{d}}(\dot{\boldsymbol{u}}) \in \mathbb{R}^{N\times 1}$ are rarely known *a priori*. ii) A perfect force appropriation denoted by Eq.(11) demands spatially-distributed, multi-harmonic forces $\boldsymbol{p}(t) \in \mathbb{R}^{N\times 1}$ to balance out the internal damping at each DOF of the test structure. It would demand a prohibitively large number of output channels of the vibration controller and inevitably result in excessive structure-shaker interactions. Fortunately, in case of a lightly-damped structure and the absence of internal resonance, a single-harmonic appropriated force is sufficient to isolate a NNM with satisfactory accuracy [9], which is known as an *imperfect force appropriation* technique [12]. In this technique, an imperfect appropriated force is applied to a single point of the structure [9-12] or at its base [13], with the applied force being tuned in quadrature (a phase lag of 90°) with respect to the fundamental displacement/acceleration response. The 90° phase lag is referred to as the *local phase quadrature criterion* [12].

The proposed strategy considers applying an imperfect appropriated force - a single-point, single-harmonic force - to the test structure:

$$\boldsymbol{p}(t)=\mathrm{Re}\left(\boldsymbol{l}_k p_{\mathrm{appr}} e^{\mathrm{j}\tilde{\omega}_r t}\right), \tag{12}$$

where $\boldsymbol{l}_k$ is the $k$-th vector, indicating the location of the applied force and $p_{\mathrm{appr}}$ denotes its magnitude.

The structural response of an arbitrary $s$-th coordinate can be denoted as:

$$u_s(t) \approx \mathrm{Re}\left(\sum_{n=0}^{N_h} \tilde{\psi}_{rs}^{(n)} e^{\mathrm{j}n\tilde{\omega}_r t}\right) = \mathrm{Re}\left(\sum_{n=0}^{N_h} \boldsymbol{l}_s^{\mathrm{T}} \tilde{\boldsymbol{\phi}}_r^{(n)} q_r e^{\mathrm{j}n\tilde{\omega}_r t}\right), \tag{13}$$

where $\psi_{rs}^{(n)}$ denotes the amplitude of responses at resonance, $\boldsymbol{l}_s$ is the $s$-th unit vector. Many papers choose the original point (i.e., $s$=$k$) to formulate the local phase quadrature criterion [9-17], while in this paper, it is generalised to an arbitrary point represented by the $s$-th coordinate ($u_s$). The driving frequency that achieves NNM isolation ($\tilde{\omega}_r$) is directly taken as the nonlinear modal frequency.

Although the use of an imperfect appropriated force is generally 'believed' to be sufficient to isolate a NNM [9], *a posteriori* check of the actual quality of the appropriation should be performed by using experimentally measured data [9,19]. In a full-field test setting, the authors recommend using indicators such as the average response function, average force function, and a full-field phase-lag map [19] to evaluate the quality of NNM isolation.

### D. Extract Nonlinear Modal Parameters

The proposed strategy estimates the nonlinear modal parameters from phase resonance and phase separation tests. The derivations of nonlinear modal frequency, modal damping ratio, and mode shapes are now detailed.

**i.** Nonlinear modal frequency

Backbone curves are used to describe the amplitude-dependent modal frequencies of a nonlinear structure. In the literature, there are two definitions of backbone curves that are experimental observable [37]. The first is the amplitude resonance definition used by Nayfeh [38], where a backbone is taken as a curve of maximal periodic response amplitude as a function of its corresponding driving frequency. The second definition, which is the one adopted in the proposed strategy, is based on the concept of phase resonance. In this definition, a backbone curve is treated as the frequency-response relationship of the unforced limit of an undamped nonlinear system [38,39]. More specifically, this backbone is experimentally approximated by a curve depicting the magnitude of the fundamental harmonic response $\tilde{\psi}_{rs}^{(1)}$ as a function of the driving frequency ($\tilde{\omega}_r$) of the appropriated force. The phase lag between the fundamental harmonic of the displacement/acceleration responses and the driving force along the backbone curve must be controlled as close as possible to 90° in the test.

**ii.** Nonlinear modal damping ratio

Extracting the nonlinear damping ratio has always been challenging in dynamic testing. In a nonlinear phase resonance test setting, researchers have proposed using the excitation power quantity [11-13], which involves calculations of active power and mass-normalised modal shapes. Herein, an alternative approach that does not involve power quantity calculations is derived for the proposed strategy.

The proposed approach first takes advantage of the mature and robust experimental modal analysis techniques to estimate modal parameters of the underlying linear system of the test structure. This is achieved by performing conventional phase separation testing techniques. Specifically, linear FRFs in the vicinity of the *r*-th mode are measured by exciting the system with very low amplitude excitations in order to avoid activating nonlinear dynamics. Subsequently, the natural frequency $\hat{\omega}_r$ and modal damping ratio $\hat{\zeta}_r$ of the underlying linear system are obtained using curve-fitting methods or the half-power bandwidth method [40]. In this regard, the underlying linear modal parameters also satisfy Eq. (9), i.e.

$$2\mathrm{j}\hat{m}_r\hat{\omega}_r^2\hat{\zeta}_r\hat{q}_r = \hat{\psi}_{rk}\hat{p}_{\mathrm{lin}}, \tag{14}$$

where the underlying linear modal parameters are denoted using the notion $\hat{\bullet}$. The modal damping ratio is $\hat{\zeta}_r = \hat{c}_r / 2\hat{m}_r\hat{\omega}_r$, and $\hat{\psi}_{rk} = \boldsymbol{l}_k^{\mathrm{T}}\hat{\boldsymbol{\psi}}_r$. $\hat{p}_{\mathrm{lin}}$ is the magnitude of the external force used to excite the system during the linear experimental modal analysis.

Next, the proposed strategy estimates the NNM damping ratios using the response data along the backbone curves. Considering the phase resonance condition of $r$-th NNM and defining an analogous expression of nonlinear damping ratio $\tilde{\zeta}_r = \tilde{c}_r / 2\tilde{m}_r\tilde{\omega}_r$, the imaginary part of Eq. (9) that describes the backbone curve of fundamental responses becomes:

$$2\mathrm{j}\tilde{m}_r\tilde{\omega}_r^2\tilde{\zeta}_r\tilde{q}_r = \tilde{\psi}_{rk}^{(1)}\tilde{p}_{\mathrm{appr}}, \tag{15}$$

where $\tilde{\psi}_{rk}^{(1)} = \boldsymbol{l}_k^{\mathrm{T}}\tilde{\boldsymbol{\psi}}_r^{(1)}$. It indicates that the imperfect appropriated force balances the equivalent modal viscous damping forces when projected to the $r$-th NNM coordinate. It is shown that mass-normalisation of the mode shapes is not strictly required at this step. Note also that the derived Eq. (15) in this paper is essentially equivalent to balancing the excitation power with the dissipative power if both sides of the equation are multiplied by the velocity term [11,12].

Comparing Eq. (15) to Eq. (14), and introducing a set of non-dimensional numbers $\bar{\zeta}_r = \tilde{\zeta}_r / \hat{\zeta}_r$, $\bar{\psi}_{rk} = \tilde{\psi}_{rk}^{(1)} / \hat{\psi}_{rk}$, $\bar{p}_{\mathrm{appr}} = \tilde{p}_{\mathrm{appr}} / \hat{p}_{\mathrm{lin}}$, $\bar{m}_r = \tilde{m}_r / \hat{m}_r$, $\bar{\omega}_r = \tilde{\omega}_r / \hat{\omega}_r$, $\bar{q}_r = \tilde{q}_r / \hat{q}_r$ denoted by the notion $\bar{\bullet}$, it leads to the expression of non-dimensional damping ratio:

$$\bar{\zeta}_r = \bar{\psi}_{rk}\bar{p}_{\mathrm{appr}} / \bar{m}_r\bar{\omega}_r^2\bar{q}_r\ . \tag{16}$$

Eq. (16) clearly shows that the nonlinear damping ratio is linked to the underlying linear damping ratio and other modal parameters. To extract nonlinear damping using Eq. (16), further assumptions of the nonlinear mode shapes are made:

Scenario 1: The fundamental mode shape of a NNM is dependent on vibration amplitudes. In case the fundamental mode shape of a NNM changes significantly with the vibration amplitudes, it is necessary to measure a set of points, including the driving point ($k$-th coordinate) and several other points distributed across the surface of the test structure. These points allow us to quantify the changes in vibration shapes. The coordinates of these measured points are then denoted as $s=\{k,\ s_1, s_2, \cdots s_{\exp}\}$. To estimate the mass matrix of the test structure, the underlying linear mode shapes are used [12,35]:

$$\mathbf{M}_{\exp} = \left(\hat{\boldsymbol{\phi}}_r^{\mathrm{T}}\right)^{+} \mathbf{I} \left(\hat{\boldsymbol{\phi}}_r\right)^{+}, \tag{17}$$

which can then be used for the normalisation of the nonlinear mode shapes [12,35]:

$$\left(\tilde{\boldsymbol{\phi}}_r^{(1)}\right)^{\mathrm{T}} \mathbf{M}_{\exp} \tilde{\boldsymbol{\phi}}_r^{(1)} = \mathbf{I}. \tag{18}$$

Note that the nonlinear mode shape is normalised using its fundamental harmonic - $\tilde{\boldsymbol{\phi}}_r^{(1)}$ - in Eq. (18).

Recall that the structural response is assumed to be dominated by one NNM, such that:

$$\bar{\psi}_s \approx \bar{\psi}_{rs} = \bar{\phi}_{rs}\bar{q}_r, \tag{19}$$

where the non-dimensional numbers $\bar{\psi}_s = \tilde{\psi}_s^{(1)} / \hat{\psi}_s$, $\bar{\phi}_{rs} = \tilde{\phi}_{rs}^{(1)} / \hat{\phi}_{rs}$ are defined similarly as those shown in Eq. (16).

Inserting Eq. (19) into Eq. (16), the nonlinear modal damping ratio can be estimated via the non-dimensional responses of an arbitrary point $\bar{\psi}_s$ (denoted by $s$-th coordinate):

$$\tilde{\zeta}_r \approx \frac{\bar{\phi}_{rk}\bar{\phi}_{rs}\bar{p}_{\mathrm{appr}}}{\bar{\omega}_r^2\bar{\psi}_s}\hat{\zeta}_r, s=k,\ s_1, s_2, \cdots s_{\exp} \tag{20}$$

For example, using the driving-point data, one obtains: $\tilde{\zeta}_r \approx \left(\bar{\phi}_{rk}^2\bar{p}_{\mathrm{appr}} / \bar{\omega}_r^2\bar{\psi}_k\right)\hat{\zeta}_r$. Note that the underlying linear damping ratio $\hat{\zeta}_r$ has already been estimated using the established experimental modal analysis techniques.

Scenario 2: The fundamental mode shape of a NNM is independent on vibration amplitudes. For a wide range of industrial structures such as turbine blades [13] or jointed structures [41], the fundamental mode shape of a NNM may remain unchanged with increasing vibration amplitudes despite substantial deviations of modal frequencies and damping ratios occur. These behaviours are often observed for structures that do not experience strong nonlinear modal interactions. In such cases, the nonlinear modal damping ratios can be extracted in a much simpler way.

Using the assumption that the fundamental nonlinear mode shape does not change with vibration amplitudes, mass-normalisation of the mode shapes becomes unnecessary since the non-dimensional numbers satisfy $\bar{\phi}_{rk} \approx 1, \bar{\phi}_{rs} \approx 1, \bar{m}_r \approx 1$. Substituting these approximations into Eq. (16), one obtains:

$$\tilde{\zeta}_r \approx \frac{\bar{p}_{\mathrm{appr}}}{\bar{\omega}_r^2 \bar{\psi}_s} \hat{\zeta}_r, \tag{21}$$

where the non-dimensional values of the appropriated force $\bar{p}_{\mathrm{appr}}$, appropriated forcing frequency $\bar{\omega}_r$, and the resonant response magnitude $\bar{\psi}_s$ can be obtained directly from the backbone curve. Eq. (21) is quite useful for extracting modal damping ratios along the backbone curve by using the response of an arbitrary point (denoted as the *s*-th coordinate). Therefore, one measuring point with a larger vibration amplitude and a better signal-to-noise ratio can be chosen in this regard.

**iii.** Full-field mode shapes

The full-field mode shapes are experimentally approximated by sinusoidal Operating Deflection Shapes (ODSs) at the phase resonance of the NNM. To allow this approximation, three conditions must be met [42]: 1) the excitation force should not be applied to nodal DOFs of the NNM, 2) the phase resonance condition must be met with sufficient accuracy, and 3) only one NNM should dominate the vibration of the test structure.

In the proposed nonlinear modal testing strategy, the full-field, multi-harmonic ODSs - $\tilde{\psi}_r^{(n)}\left(n=1\cdots N_h\right)$ - are obtained by performing a series of sine-dwell tests, in which the driving force dwells at few discrete frequencies along the backbone curve for a certain duration while the 3D SLDV measures the corresponding full-field vibrations. To reduce testing time, a super-short sampling interval is used for each scan point, resulting in a coarse frequency resolution and severe spectral leakages in the response spectra, as expected. A multi-step Interpolated-FFT algorithm proposed by the authors [18,19] is therefore recommended to refine the frequency resolution and reduce energy leakages.

## E. Synthesis of Near-resonant Frequency Responses

Under the assumption of single-NNM motion expressed by Eq. (9), the nonlinear modal parameters can be used to synthesise the near-resonant forced responses. This is achieved by expressing the driving frequency as a function of the magnitudes of the appropriated force [1,2, 13], i.e.

$$\Omega_{\pm}^2 = \Gamma_\omega \pm \sqrt{\Gamma_\omega^2 - \tilde{\omega}_r^4 + \tilde{\alpha}^2 \left(\tilde{p}_{\mathrm{appr}} / \tilde{\psi}_s^{(1)}\right)^2}, \tag{22}$$

where $\Gamma_{\omega}=\tilde{\omega}_r^2-2\tilde{\zeta}_r^2\tilde{\omega}_r^2$, and $\tilde{\alpha}=\tilde{\phi}_{rk}^{(1)}\tilde{\phi}_{rs}^{(1)}/\tilde{m}_r$. $\tilde{\psi}_s^{(1)}$ denotes the fundamental responses of the $s$-th coordinate.

Substituting the nonlinear modal parameters into Eq. (22), the driving frequencies $\Omega$ can be resolved for given response amplitudes, thereby obtaining the nonlinear responses explicitly [43,44]. In the case of NNM mode shape that is independent of vibration amplitudes, $\tilde{\alpha}$ can be approximated by its underlying linear value without mass-normalisation, i.e.

$$\tilde{\alpha}\approx\hat{\alpha}=2\tilde{\zeta}_r\hat{\omega}_r^2\hat{\psi}_s/\hat{p}_{\mathrm{lin}}. \tag{23}$$

Eq. (22) is often used to validate the accuracy of the extracted nonlinear modal parameters by comparing its synthesised frequency responses to the directly measured ones [2]. Note that the synthesis could be extended to include multi-harmonic terms of the resonant mode and contributions of the off-resonant modes if necessary [34].

# III. Full-field measurement strategy

## A. Test Setup

Figure 1 illustrates the proposed test setup for full-field measurement of lightweight nonlinear structures. It combines a 3D SLDV with a MISO vibration controller. The controller applies phase separation and phase resonance testing techniques to the structure, while the 3D SLDV carries out full-field measurements when the controller reaches a steady state. The 3D SLDV measures three-dimensional vibration responses of a scan point at a sampling rate that should be at least twice the highest constituent harmonic of interest. Figure 1 shows that the two systems are synchronised via the excitation force signal applied to the structure. This signal is simultaneously sampled by the MISO vibration controller (for the purpose of closed-loop control) and the 3D SLDV (as a reference). An accelerometer is attached to the tip of the test structure for closed-loop control, and its signal is used to define a vibration limit to ensure structure safety.

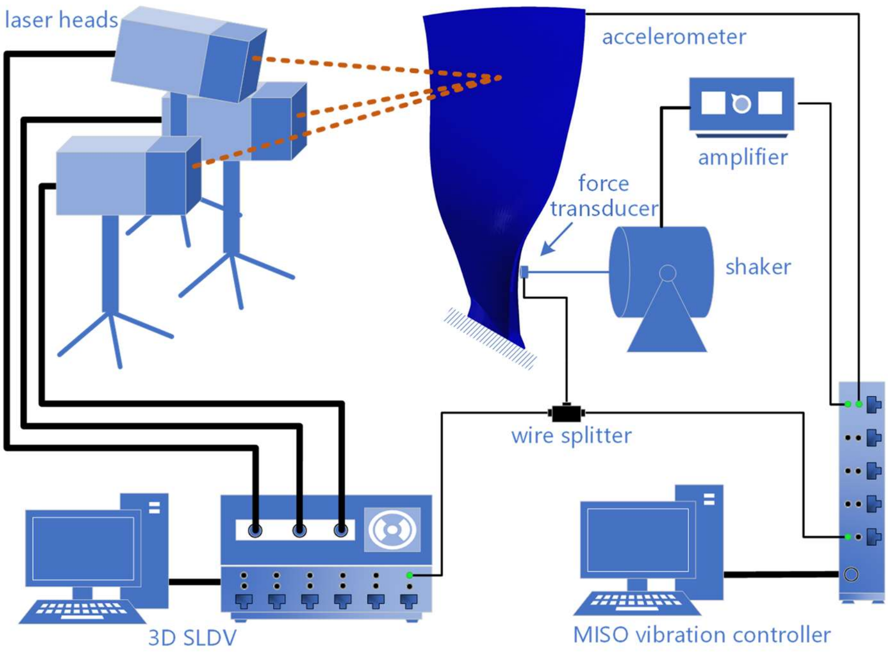


Figure 1. Proposed test setup for full-field measurement of lightweight structures.

## B. Proposed Test Strategy

Figure 2 depicts a flow chart that outlines three main phases of the proposed full-field nonlinear modal testing strategy. Phase I involves applying low-amplitude excitations to the test structure and conducting conventional linear modal testing to estimate the underlying linear modal parameters. In Phase II, the lack of homogeneity of FRFs is used to detect NNMs first, followed by performing nonlinear modal testing for each detected NNM. To reduce the overall testing time, phase separation and phase resonance testing techniques are integrated in this phase. The measured nonlinear modal parameters are also validated at the end of Phase II. Finally, in Phase III, the test structure undergoes an integrity check. A few key details are highlighted as follows:

Phase I applies conventional full-field linear modal testing techniques to the structure and obtains modal parameters of its underlying linear model [45]. In Step 1, FRFs of a few representative points (avoiding nodal points) are firstly measured using low-amplitude excitations. It is then followed by applying the conventional experimental modal analysis algorithms [40] to the measured FRFs and extracting linear natural frequencies and modal damping ratios within the frequency range of interest. It is worth noting that a relatively long sampling interval for each representative point should be used to allow a fine frequency resolution of the FRFs. This would not take too much time since only a limited number of representative points are measured at this stage. Step 2 utilises the identified linear natural frequencies and measures linear resonant operating deflection shapes (ODSs) using the so-called 'Fast-Scan' mode of the 3D SLDV [46]. This manner allows measurement of the responses at a speed of up to 50 scan points per second.

During Phase II, the full-field nonlinear modal testing is carried out. It starts with Step 3 of exciting the test structure with a slowly swept-sine force at a much higher input level than the initial linear response measurements to trigger nonlinear dynamic behaviours. Then, simple indices such as resonance frequency shifting can be used to ascertain the modes containing non-trivial nonlinearity; this step is frequently referred to as the 'detection' of NNMs in the literature [45,47,48]. It is followed by Step 4, in which a fast nonlinear phase resonance test is performed to trace out the backbone curve of a NNM using low to high input levels. During this step, dedicated forcing signals generated by PLL controllers [11-13], CBC methods [14-17], or resonance tracking techniques [18,19] can be adopted. Additionally, only a few representative points are measured to reduce testing time. Using the test data gathered in Step 4, the nonlinear modal frequencies and damping ratios are estimated along the backbone curve. Step 5 then applies the nonlinear phase resonance testing technique to the test structure but only dwells at a few forcing levels for a period of time (sine-dwell testing), while the 3D SLDV is used to measure the full-field responses of the vibrating structure. To reduce testing time, a super-short sampling interval is used for each scan point. Thereafter, the Multi-step Interpolated FFT algorithm [19] is applied to the measured spectra to refine the frequency resolutions and remove the unwanted energy leakages, obtaining multi-harmonic full-field ODSs with improved accuracy. As shown in Figure 2, Phase II ends up with Step 6 of validation. In this step, mini-sweeps around the NNMs are performed, and the near-resonant frequency responses at a few high-amplitude forcing levels are measured. These directly measured frequency responses are reserved for validating the extracted modal parameters of NNMs. It is important to note that Steps 4 to 6 should be applied to each detected NNM of the test structure sequentially until all the NNMs are measured.

Phase III performs a final check of the test structure by applying the same low-amplitude excitation as Phase I. The resulting FRFs are then compared to those obtained during Phase I. This ensures that the test structure does not have noticeable changes in dynamics after the high-amplitude test campaign.

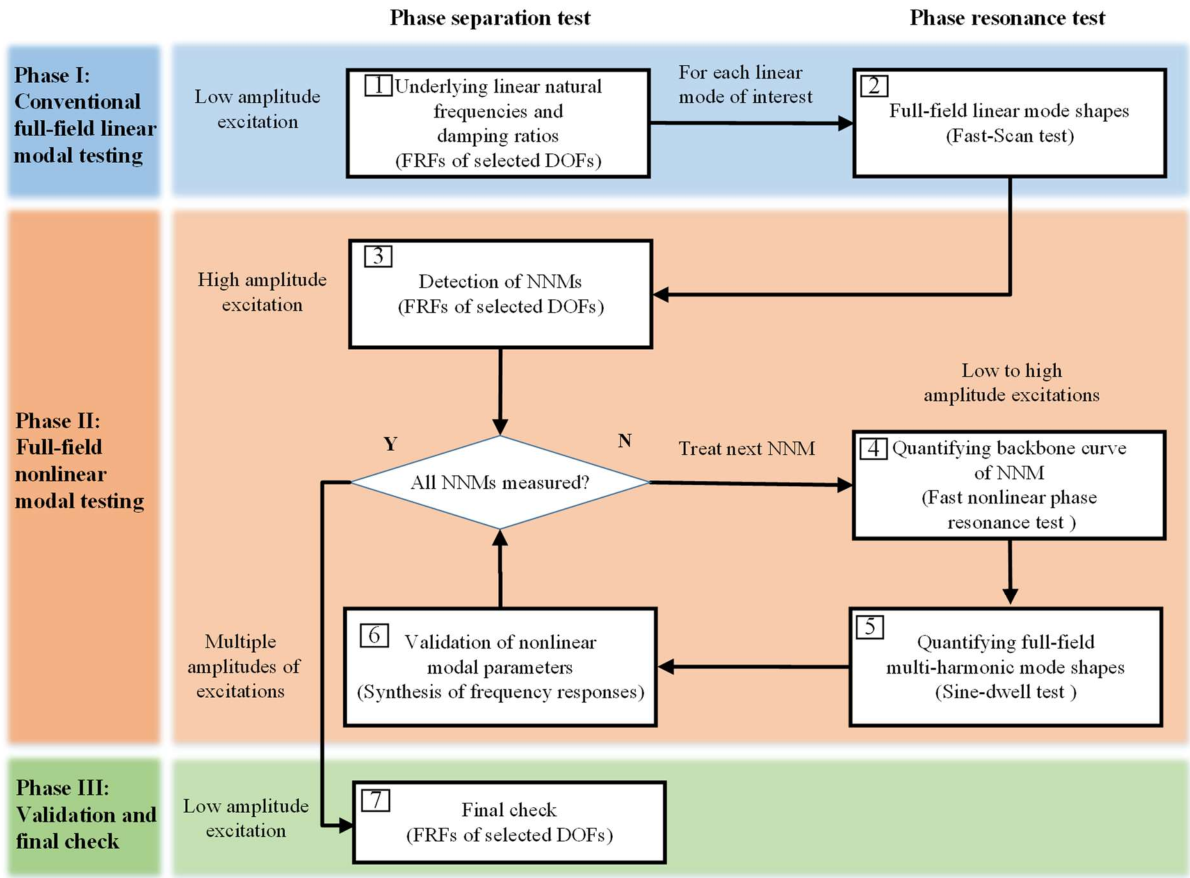


Figure 2. The proposed full-field measurement strategy for lightweight nonlinear structures.

## IV. Application to an aero-engine fan blade

The proposed test strategy is explained in detail in this section, using a realistic, full-scale fan blade as an example. As shown in Figure 3, the investigated fan blade was clamped at the root. At the back side of the blade, a single-point input force was applied near the root of the blade by a Data Physics Signal Force V4 shaker. The shaker was controlled by a MISO vibration controller (Data Physics SignalStar ABACUS Vector). The applied force was measured via a PCB 208C02 transducer, and the response of the blade tip (also referred to as a monitoring point) was measured by a triaxial accelerometer (PCB 356A03). The 3D SLDV used for the test was a Polytec PSV-500-3D-HV Scanning Laser Doppler

Vibrometer. Figure 3 also illustrates the dense measurement grid defined on the blade's front surface. It consists of as many as 2016 scan points. The test setup was initially prepared for a technology demonstration, which could be further improved in many aspects: 1) use a non-contact magnetic shaker to replace the Data Physics Signal Force V4 shaker, or 2) adopt a laser Doppler vibrometer (LDV) instead of the attached accelerometer to measure the blade's tip responses. However, these improvements are beyond the scope of this paper. Note also that the test results of the fan blade are normalised for commercial confidentiality reasons.

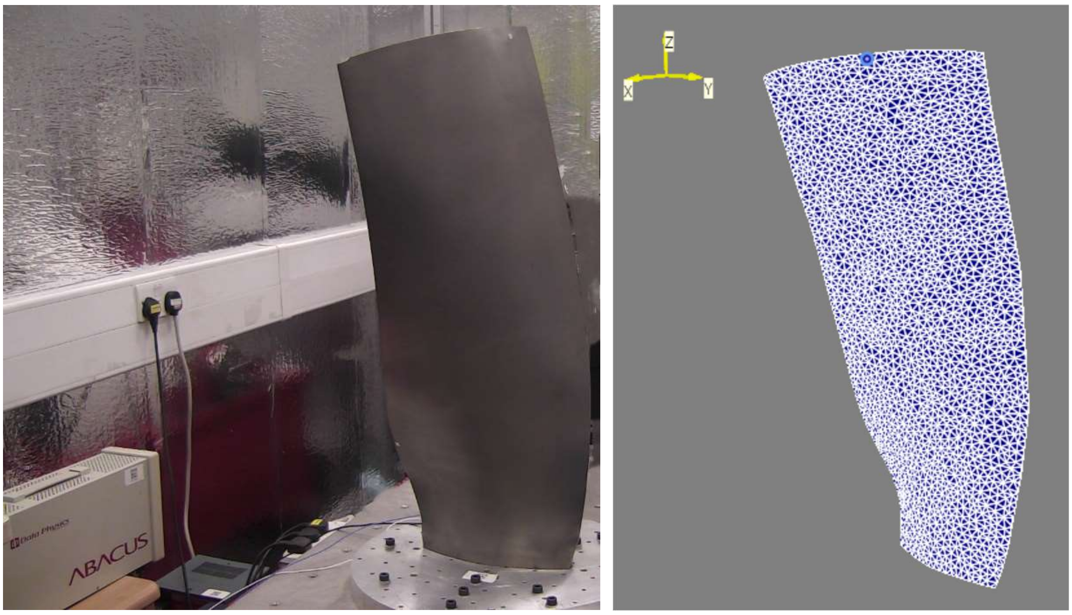


Figure 3. A picture of the fan blade test setup, in which the white dots represent scan points.

### A. Phase I: Full-field Linear Modal Testing

In Phase I, A conventional full-field linear modal test was conducted first to estimate the underlying linear modal parameters of the test structure. This phase involves two steps: the first step is to identify natural frequencies and damping ratios, and the second step is to measure full-field mode shapes.

In Step 1, to obtain the underlying linear natural frequencies and damping ratios of the blade, an open-loop, low-amplitude random signal was used to drive the shaker and the Single-Shot measurement mode of 3D SLDV was employed to measure FRFs of three representative points - TipLeft, TipMiddle, and TipRight, as shown in Figure 4. The FRFs were measured at a sampling frequency of 2.5 kHz, and 102400 spectral lines were set in the frequency range of 0-1000 Hz, providing a very fine frequency resolution of 9.77 mHz. Figure 5 depicts the measured FRF curves of the representative points, with each curve being estimated using five peak-hold averages to mitigate the noise effect. To verify if the low-amplitude forcing excites linear responses, a slightly higher-level random force was applied to the structure and the FRFs were measured again. A comparison between the initial and the second test results shows no recognisable variations in the measured FRF, affirming that the initial measured dynamics can be considered linear. Consequently, the initial FRFs of the representative points in the x- and y- directions, as plotted in Figure 3, were used to extract the underlying linear modal parameters of the blade. Note that the z-directional (axial direction of the fan blade) responses were too small and hence excluded in the modal analysis.

Figure 6 shows the stabilisation diagram obtained by applying the least-squares rational function estimation method [49] to the measured linear FRFs. The stable criterion is set to 0.5% for the frequency and 1% for the damping ratio. In the diagram, the fitting model order is set to 18, and 14 stable modes are observed within the frequency range of interest. Table 1 lists the identified linear natural frequencies and modal damping ratios. Note that all presented values are normalised using the first modal parameters, as required by our industry partner.

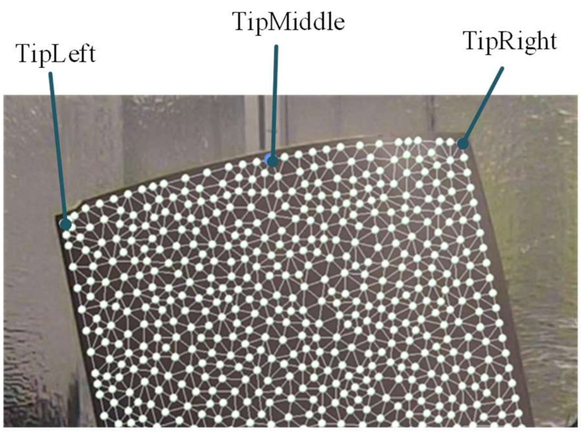


Figure 4. A zoom-in view of the three representative points.

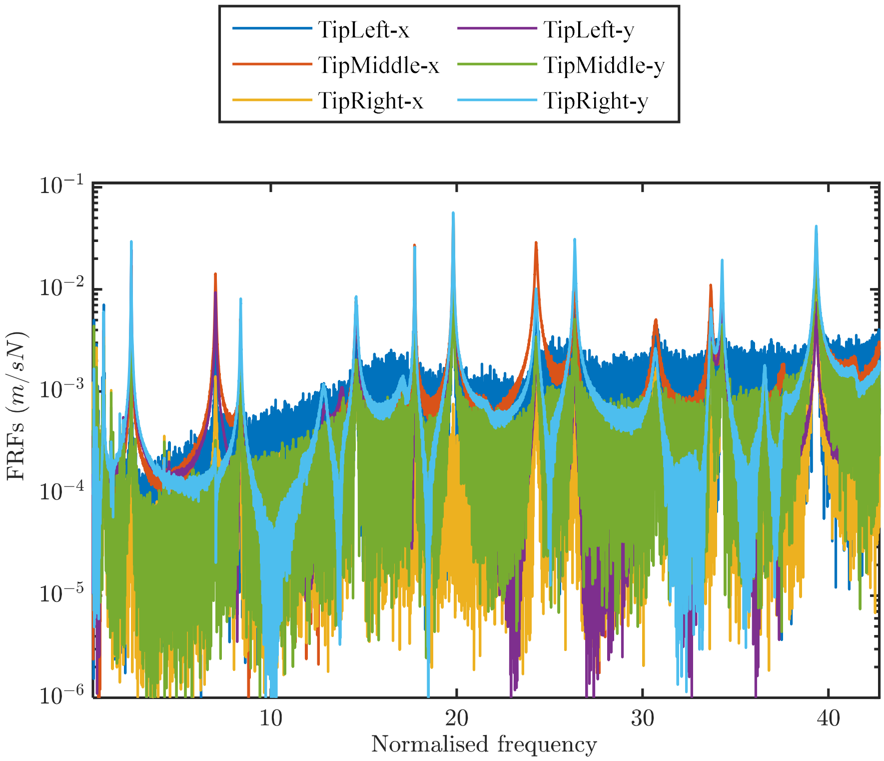


Figure 5. Measured mobility FRFs of the representative points using low-amplitude random excitations.

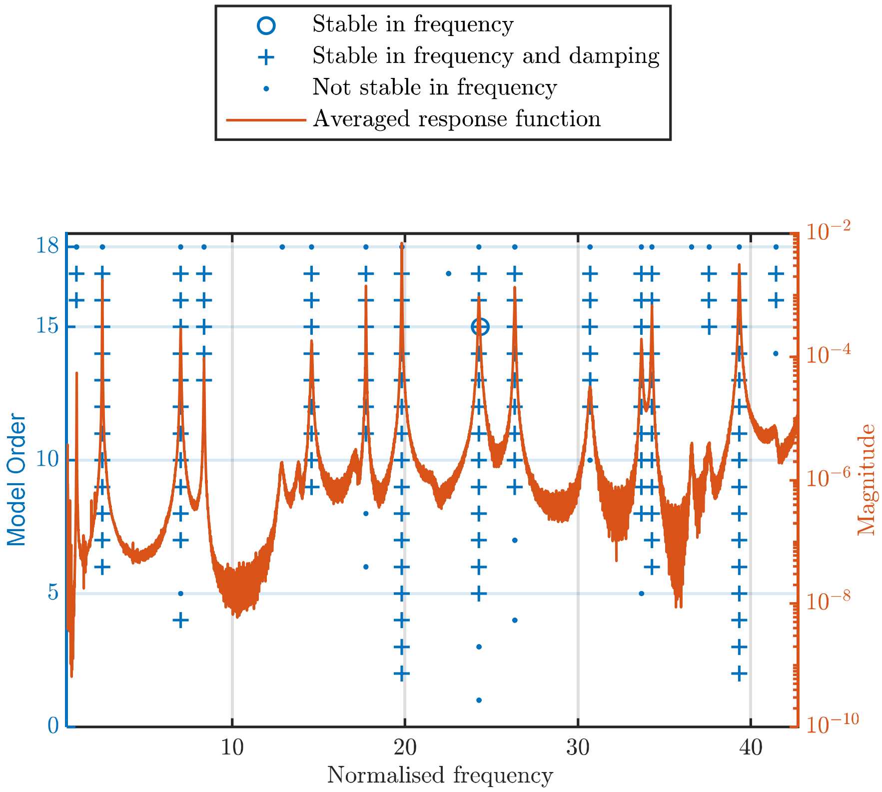


Figure 6. Stabilisation diagram of the fan blade.

Table 1. Identified underlying linear modal parameters of the fan blade.

| Mode order | 1 | 2 | 3 | 4 | 5 | 6 | 7 |
|---|---|---|---|---|---|---|---|
| Normalised natural frequency | 1 | 2.494 | 7.023 | 8.375 | 14.594 | 17.738 | 19.815 |
| Normalised modal damping ratio | 1 | 0.6 | 0.75 | 0.45 | 0.75 | 0.15 | 0.15 |
| Mode order | 8 | 9 | 10 | 11 | 12 | 13 | 14 |
| Normalised natural frequency | 24.275 | 26.352 | 30.703 | 33.672 | 34.283 | 37.584 | 39.339 |
| Normalised modal damping ratio | 0.45 | 0.23 | 0.87 | 0.30 | 0.18 | 1.00 | 0.20 |

In Step 2, the linear mode shapes are experimentally approximated by the sinusoidal ODSs at resonance [42]. In this regard, the forcing frequency was set to each identified natural frequency ( listed in Table 1), and the 3D SLDV was then switched to the Fast-Scan mode [46] to measure full-field linear ODSs. All of the 14 modes in the frequency range of interest were measured, with each measurement taking approximately 1 - 3 minutes. Six of the linear mode shapes with contour lines highlighting the vibration magnitudes are shown in Figure 7; these figures are directly provided by the Polytech Scan Viewer.

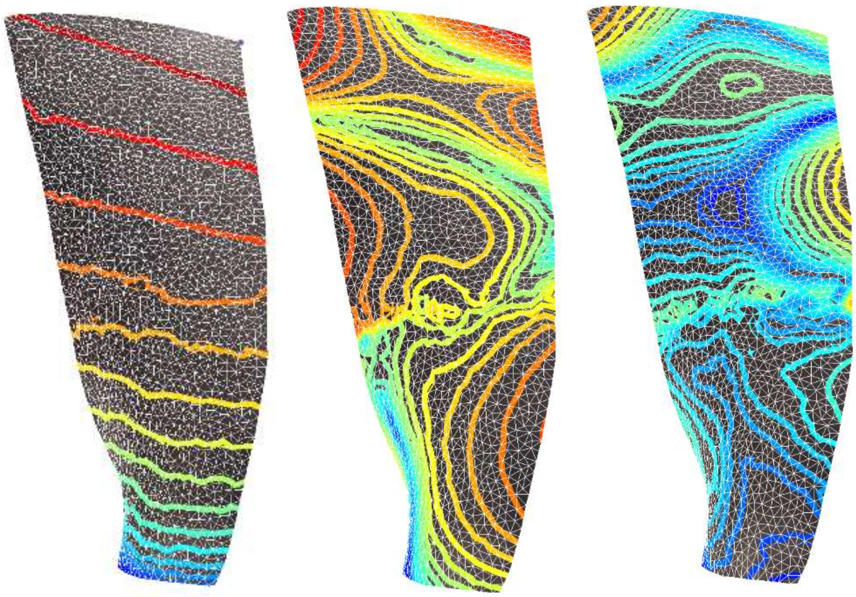

(a) (b) (c)

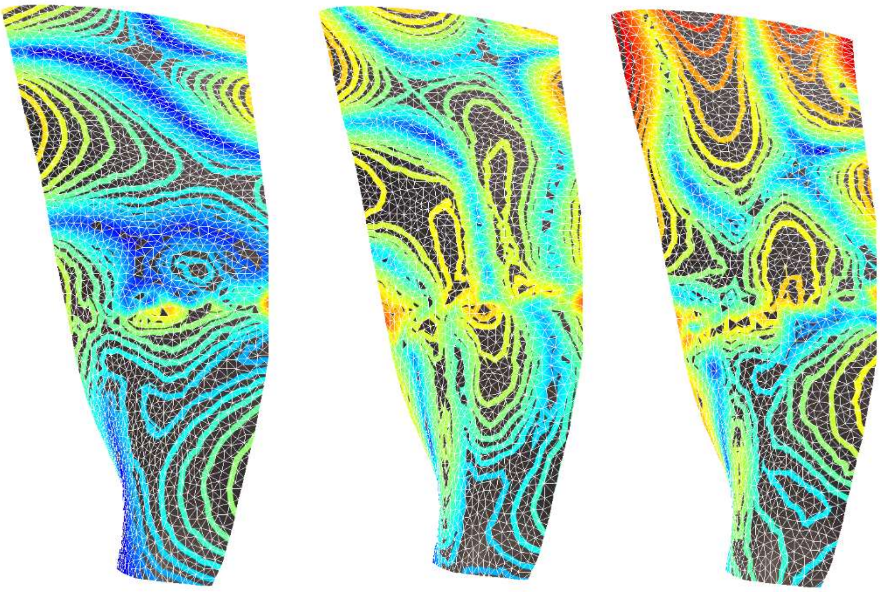

Figure 7. Six representative linear ODSs at the resonances of (a) Mode 1, (b) Mode 6, (c) Mode 8, (d) Mode 9, (e) Mode 12 and (d) Mode 14, respectively.

It is clearly shown in Figure 7 that the higher-order mode shapes are highly curved in three dimensions, with many edge-wise localised vibration patterns. This highlights the complex nature of mode shapes in industrial structures and demonstrates the high quality of full-field measurements using 3D SLDV. The underlying linear natural frequencies, damping ratios and full-field mode shapes of the fan blade have been quantified within the prescribed frequency range. The next phase would be to commence the nonlinear measurement campaign.

## B. Phase II: Full-field Nonlinear Modal Testing

During Phase II, Step 3 involves applying representative amplitudes of excitations that the structure is likely to experience in service [45]. Thereby, a much higher-amplitude excitation was applied to the fan blade, and the blade tip FRFs were measured. To detect NNMs, the FRFs are compared to those measured during Phase I using low-amplitude excitations. If there are any distortions of the peaks or a lack of homogeneity of FRFs, it would be an intuitive indication of nonlinearities [45,47,48].

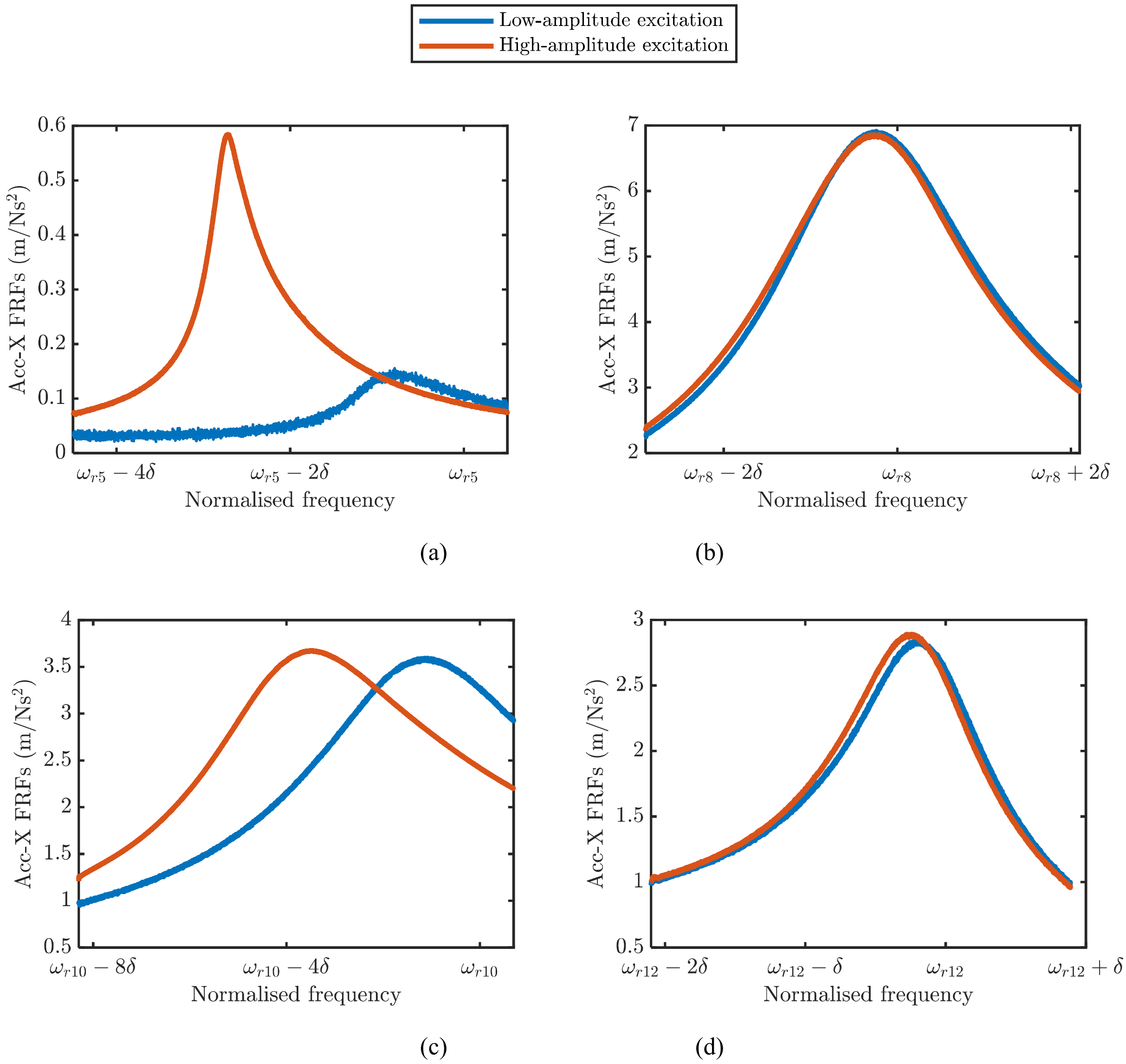


Figure 8. Comparison of the blade's tip accelerance using low- and high-amplitude excitations for (a) Mode 5, (b) Mode 8, (c) Mode 10, and (d) Mode 12.

Figure 8 presents zoom-in views of the blade tip accelerances for four representative modes of interest. Mode 5 shows a strong softening trend in stiffness and lower damping with increased excitation levels. Similarly, Mode 10 also demonstrates a stiffness softening phenomenon, but the resonance peak magnitude seems unchanged. For Modes 8 and 12, the FRF discrepancies are trivial, thus allowing them to be treated as linear modes. Here, it should be mentioned again that the thresholds of frequency shift or change of FRF resonant magnitudes for a mode to be deemed as NNM are dependent on individual industrial requirements. In this case, Modes 5 and 10 are considered NNMs, denoted as NNM 5 and NNM 10, and further investigated in the test campaign. No additional tests were conducted for Modes 8 and 12.

Next, the backbone curves of NNM 5 and NNM 10 were traced out in Step 4 using fast nonlinear phase resonance testing. In the test, the input force was controlled using a resonance tracking module provided by the Data Physics ABACUS controller, while the responses were measured by the attached monitoring accelerometer at the blade's tip. The resonance tracking module started with a low amplitude of excitation and searched for a phase resonance with user-defined accuracy of phase-lag quadrature criterion (1° was used for the fan blade). Once the resonance was reached and the data recorded, the controller automatically increased the driving force to the next pre-defined level. Using this step-wise tracking method, the entire branch of the NNM backbone curve was traced out from the low to the highest excitation amplitudes.

Figure 9 depicts the measured backbone curves of NNM 5 and NNM 10, respectively. It is shown that both curves lean towards lower frequencies as the vibration levels increased, which confirmed again that these are two modes of softening type. The starting points of the NNM backbone curves are offset from the underlying linear natural frequencies for both modes (estimated in Step 1). This indicates that weak nonlinearities are already present even using the lowest-amplitude sinusoidal input in a phase resonance test.

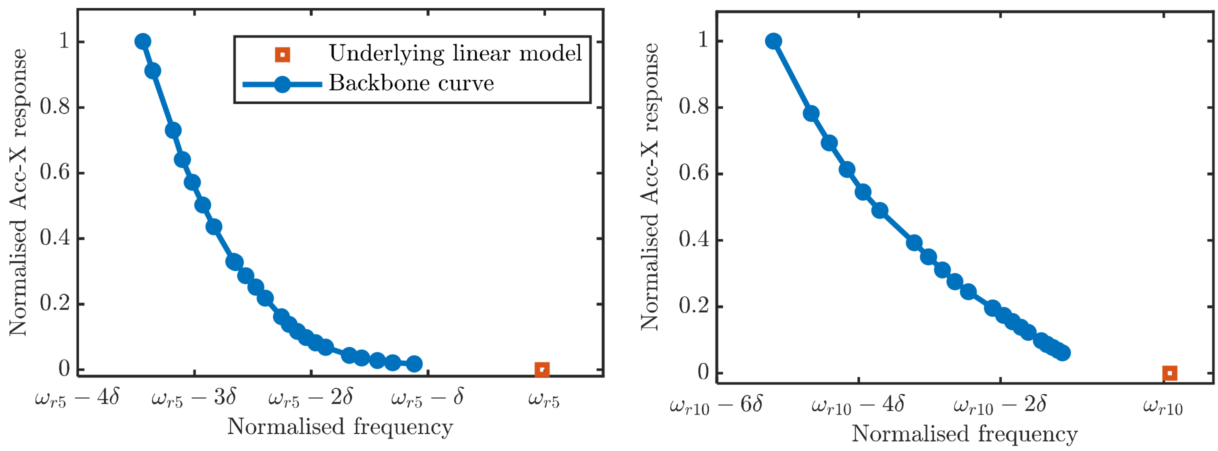


(a) (b)

Figure 9. Measured backbone curves of (a) NNM 5 and (b) NNM 10, while each dot represents a step in the fast nonlinear phase resonance test. The squares highlight the modal frequencies of the underlying linear models measured in Step 1. The response magnitudes are normalised using the peak amplitudes of each mode.

Figure 10 shows the nonlinear damping ratios estimated using Eq. (21), where the values are normalised using the corresponding underlying linear values. As can be seen, the damping ratios of the two NNMs vary with vibration levels in different trends. For NNM 5, the starting point of the backbone curve (obtained in Step 4 using the fast nonlinear phase resonance testing) is only 67% compared to the underlying linear modal damping ratio (estimated in Step 1 using phase separation testing). Figure 10(a) also shows that the nonlinear damping ratio of the backbone curve drops rapidly with increased excitation levels and reaches a stable value of only 20% compared to the underlying linear value. In contrast, as shown in Figure 10 (b), the modal damping ratio of NNM 10 remains nearly constant with increased vibration levels. Only a slight fluctuation within 6% is observed. Due to the weak damping nonlinearity, its underlying linear modal damping ratio is also close to the starting point of the backbone curve with less than 1% discrepancy.

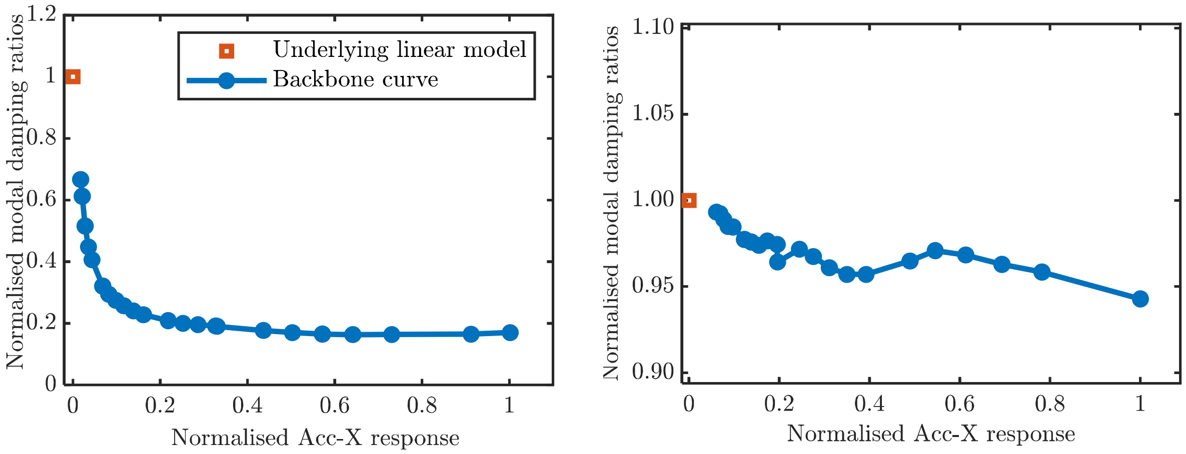


(a) (b)

Figure 10. Estimated modal damping ratios of (a) NNM 5 and (b) NNM 10. The squares highlight the damping ratios of the underlying linear models measured in Step 1. The modal damping ratios are normalised using the corresponding underlying linear damping ratios.

In the proposed strategy, the nonlinear mode shapes are experimentally approximated by sinusoidal ODSs along the backbone curve. To do this, Step 5 uses the MISO vibration controller to apply the sine-dwell test: the structure vibrates at one of its phase resonances for a few minutes, allowing the 3D SLDV to measure the steady-state full-field vibration responses. The forcing amplitude was chosen as the control target. The sampling frequency was set to 12.5 kHz for 3D SLDV, which well exceeded the highest harmonics of interest. In addition, only a duration of 0.32 s was set for each scan point, significantly reducing the overall testing time. However, such a super-short sampling time results in severe spectral leakage and coarse frequency resolution (3.125 Hz) of the spectrum. Consequently, the measured 3D SLDV datasets were post-processed with an in-house-developed multi-step Interpolated-FFT software package [19] to suppress the spectra leakages and refine the frequency resolutions of the measured results. For the fan blade test, the vibration controller dwelled at five representative vibration levels of the identified backbone curves of NNM 5 and NNM 10, respectively.

i. Full-field phase lags

The quality of NNM force appropriation is evaluated in terms of full-field phase lags, and the scan points are categorised into *Phase quadrature points*, *Non-quadrature points* and *Outliers* [19]. For each scan point, the phase-lag quadrature criterion of the x- and y-directional responses is set to $10^\circ$ to avoid oversensitivity. Note again that the z-directional responses are too small and thus not considered in data analysis.

Figure 11(a) to (e) depict the full-field phase lags at Resonances A to E of NNM 5, respectively. Figure 11(f) also displays the underlying linear mode shape of Mode 5 for a better interpretation of the distributions of non-quadrature points and outliers. It can be seen that non-quadrature points are frequently observed around nodal lines, while outliers often exist in areas with poor surface conditions (red-dotted area). As the vibration level increases, the numbers of non-quadrature points and outliers decrease dramatically, which is reasonable due to improved signal-to-noise ratios. Overall, most scan points vibrate in phase quadrature (green dots) with the input force, indicating that the modes were appropriated with satisfactory accuracy.

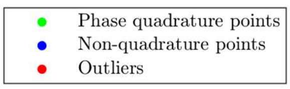

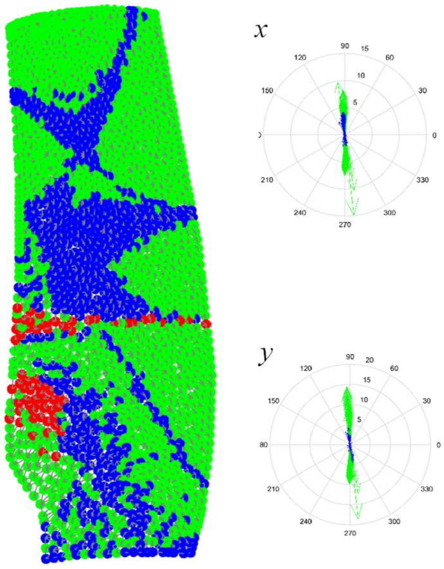


(a)

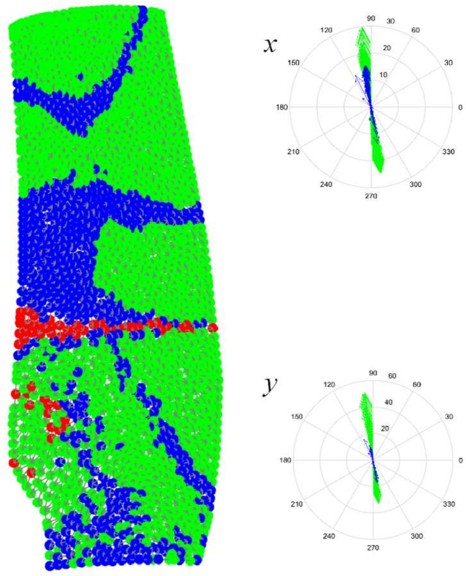


(b)

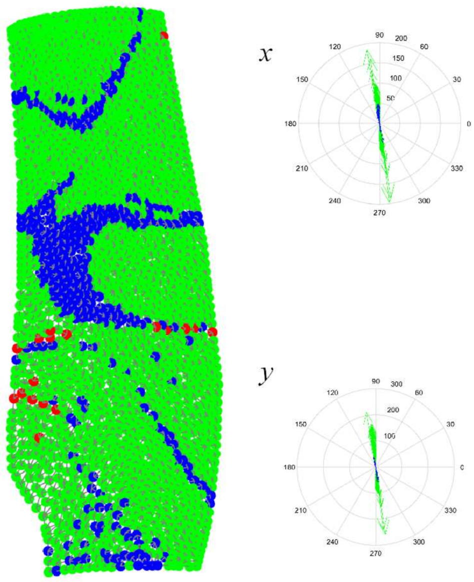


(c)

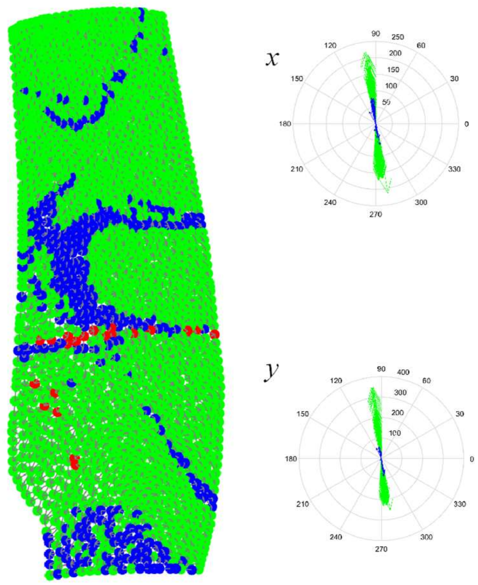


(d)

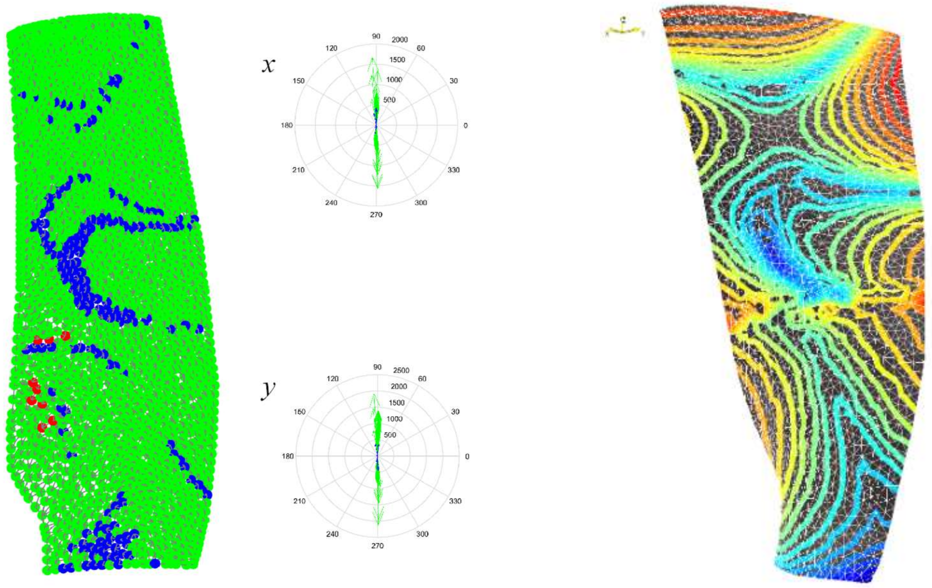


(e) (f)

Figure 11. Full-field phase lags and phase scatter diagrams of NNM 5 with increasing forcing amplitudes leading to (a) Resonance A, (b) Resonance B, (c) Resonance C, (d) Resonance D, and (e) Resonance E obtained by using the Multi-step Interpolated-FFT procedure; (f) shows the underlying linear mode shape of Mode 5.

ii. Input forces of scan points

During the test, the FFT spectrum of the input force is closely monitored for each scan point. Ideally, it should be a single sharp peak. In practice, the force spectra of all phase quadrature points are averaged to formulate the so-called *average force spectrum* [19] for a resonance, allowing visualisation of the strength of each harmonic component. Figure 12 shows the resulting average force spectra at Resonances A to E of NNM 5. In the figure, the fundamental harmonic component appears as a sharp peak in the spectrum, and the higher-order harmonics are trivial for Resonances A to D but evident for Resonance E. Specifically, Figure 12(e) shows that the third harmonic of Resonance E reaches 19.1% of its fundamental harmonic. This is attributed to shaker-structure interactions as strong nonlinear behaviours occur. Suppression of these interactions would require dedicated modelling and control efforts, which are currently being developed [50,51] but beyond the scope of this paper. It is also shown in Figure 12 that the FFT spectra of input forces only have a coarse frequency resolution of 3.125 Hz, and the magnitude estimates have discrepancies of 1.91%, 17.11%, 9.16%, 6.28% and 0.66% for Resonances A to E compared to the values provided by the MISO vibration controller. This is due to spectral leakages in the FFT spectra, which are almost guaranteed to occur when a non-integral number of signal cycles are sampled in a super-short interval.

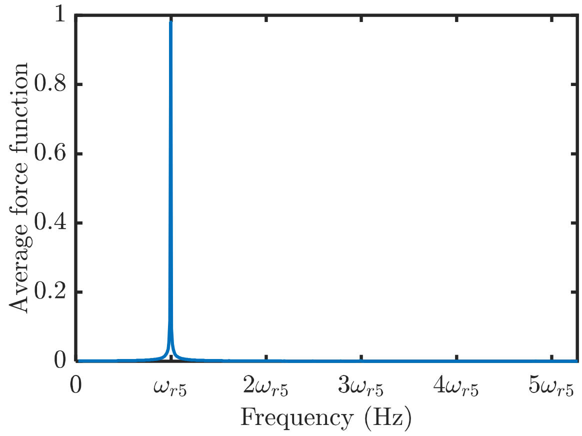


(a)

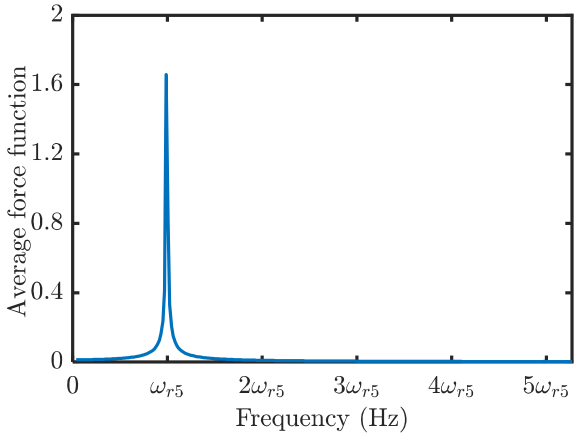


(b)

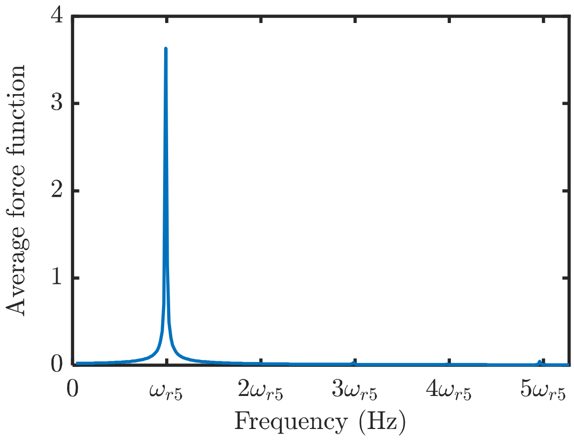


(c)

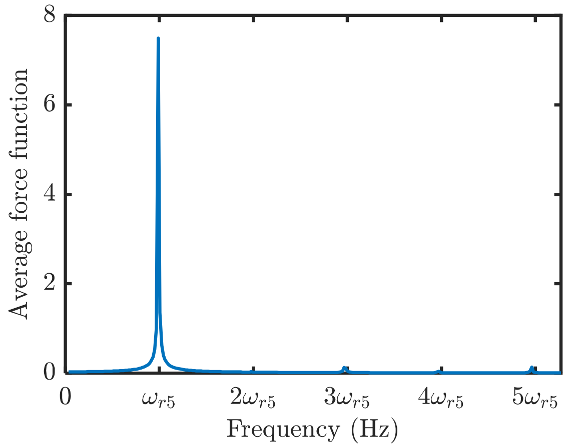


(d)

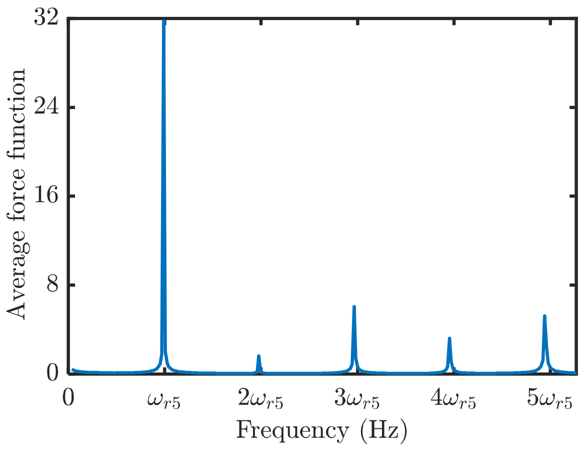


(e)

Figure 12. Average force spectra at (a) Resonance A, (b) Resonance B, (c) Resonance C, (d) Resonance D, and (e) Resonance E of NNM 5 formulated using 3D SLDV datasets. The magnitudes are normalised using the input force of Resonance A.

To suppress spectral leakage and refine frequency resolution, the 3D SLDV datasets are processed with in-house code, allowing the multi-step Interpolated FFT procedure to estimate the true frequencies and magnitudes of harmonics. Figure 13 shows the improved estimates of the fundamental harmonic forces, where the magnitudes agree quite well with the corresponding control targets set in the MISO vibration controller. The Root Mean Square (RMS) discrepancies of the input forces are now below 0.2% for all the resonances; this confirmed that the MISO controller achieved excellent force control during the test, and the multi-step Interpolated FFT procedure provides estimations with significantly improved accuracy.

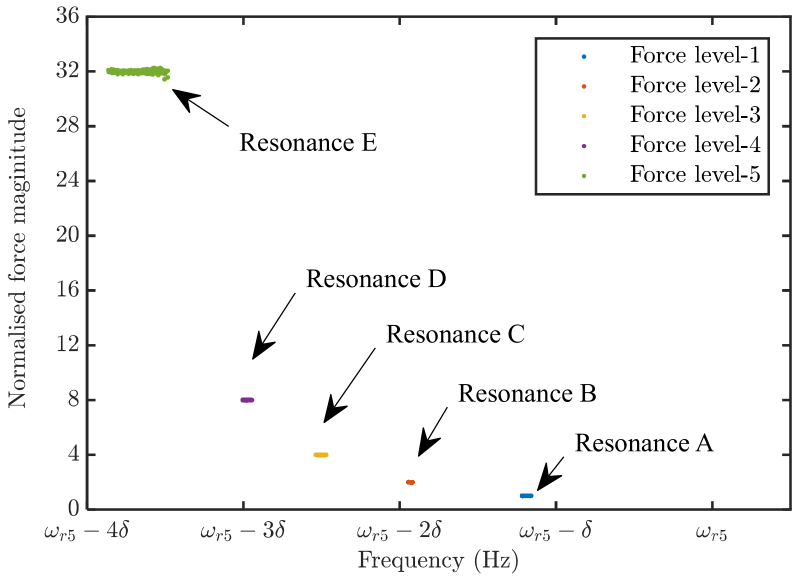


Figure 13. The appropriated force of NNM 5, where the fundamental harmonic forces were estimated by applying the multi-step Interpolated-FFT procedure to the 3D SLDV datasets. Each dot in the figure represents a scan point. The forces were normalised using the target forcing level of Resonance A.

iii. Full-field multi-harmonic mode shapes

Figure 14 shows the average response spectra [19] and the full-field mode shapes of NNM 5. The former highlights the contributions of each harmonic, and the latter visualises the corresponding deformation patterns. Despite substantial frequency shifting being found for these resonances (see Figure 13), the amplitudes of the higher-order harmonics are trivial compared to the fundamental harmonic for Resonances A to D. For Resonance E. However, the higher-order harmonics were triggered as the structure vibrated in larger amplitudes. At this resonance, clear edge-wise localised patterns of higher-order harmonic shapes are observed (see Figure 14(e)), leading to redistributions of stress concentration areas that differ from the fundamental one. It is also interesting to point out that the deformation patterns of a few higher-order harmonics resemble the fundamental component (e.g., Figure 14(a) and(b)), while others do not (e.g., Figure 14(e)). It is shown by this fan blade case that the spatially-detailed, multi-harmonic NNM shapes provided valuable information into the nonlinear dynamics.

(a)

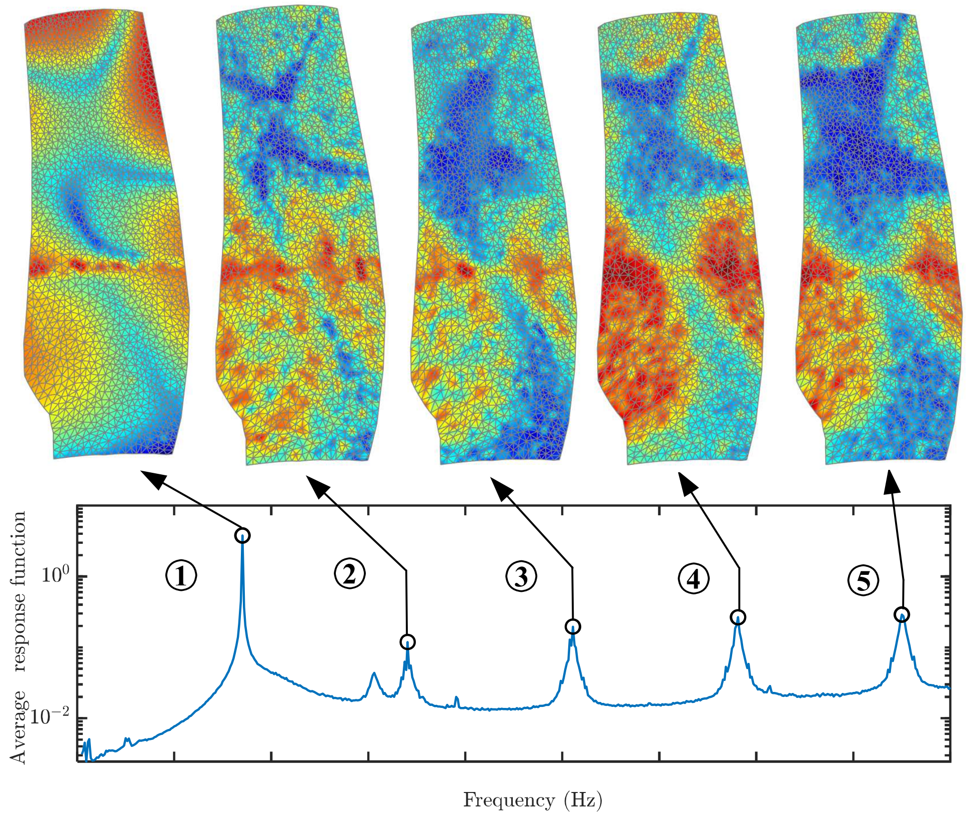

(b)

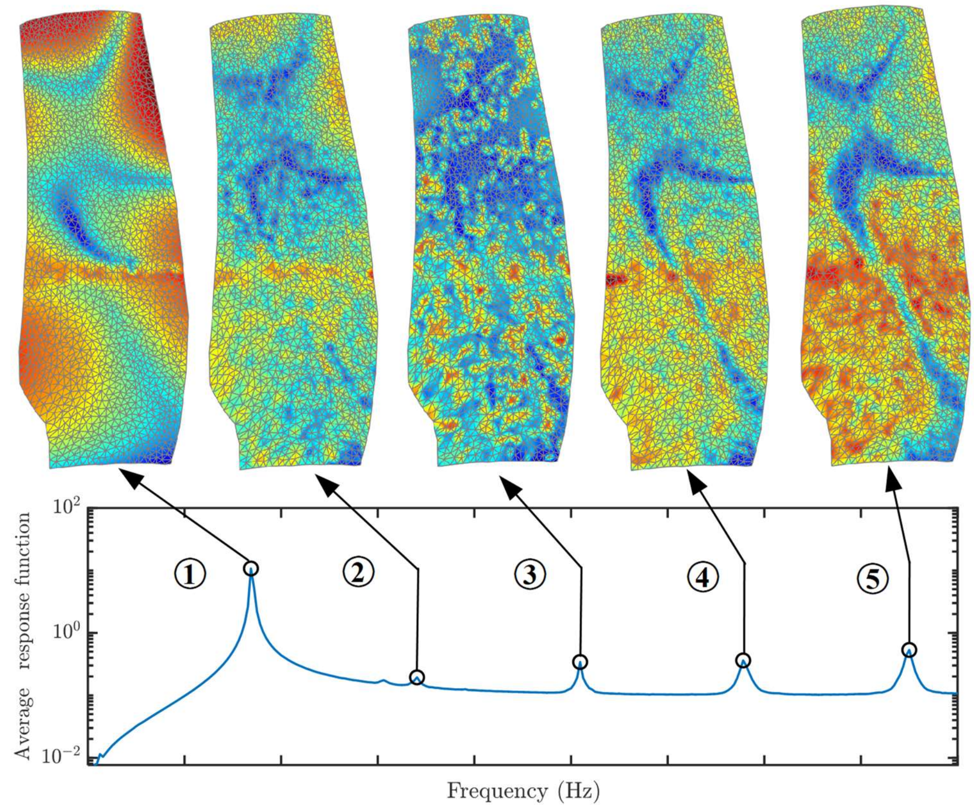

①
②
③
④
⑤
$10^2$
$10^0$
$10^{-2}$
Average response function
Frequency (Hz)


(c)

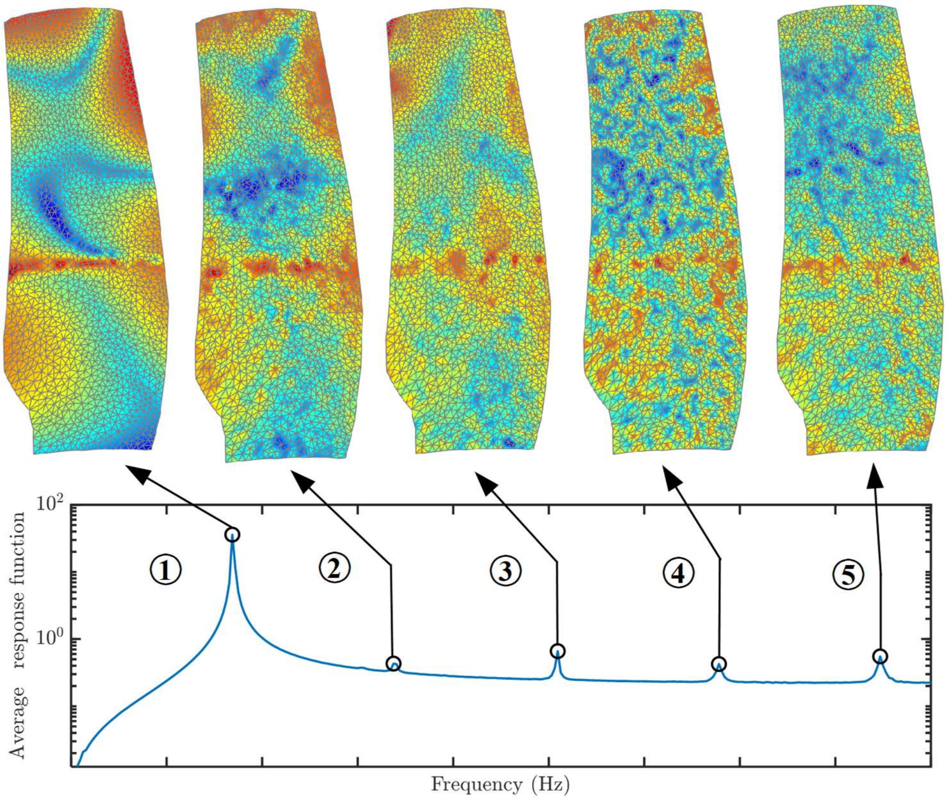

①
②
③
④
⑤
$10^2$
$10^0$
Average response function
Frequency (Hz)

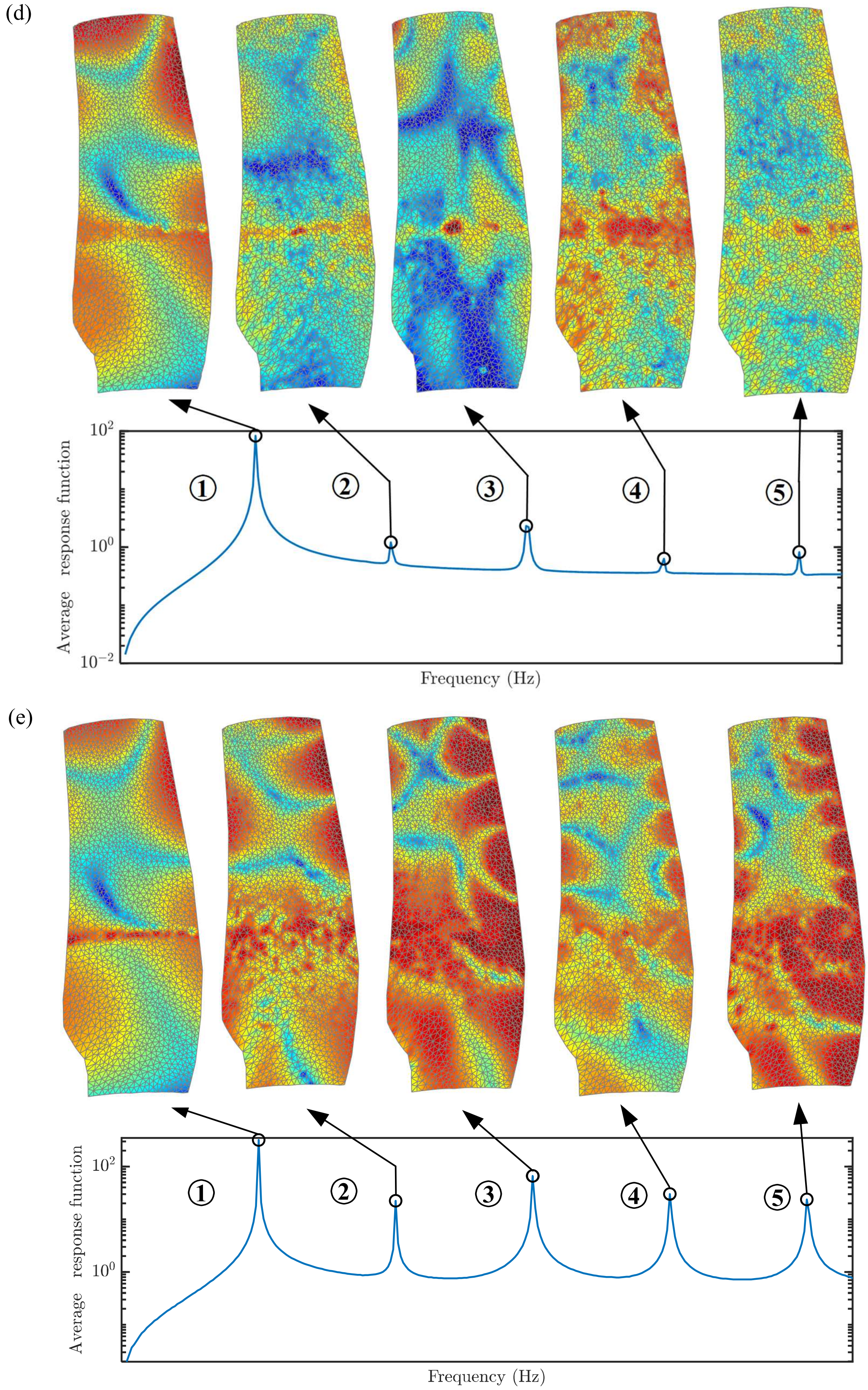


Figure 14. Full-field, multi-harmonic mode shapes at (a) Resonance A, (b) Resonance B, (c) Resonance C, (d) Resonance D and (e) Resonance E of NNM 5.

A former paper [19] aimed to investigate the multi-step Interpolated-FFT procedure published the results of NNM 10. Herein, this paper only presents the full-field results of NNM 5. Interested readers are referred to Ref [19] for detailed mode shapes of NNM 10.

After quantifying the modal parameters of the detected NNM, Step 6 directly measures the frequency responses around the NNMs using multiple input levels of sine-sweeps. At this point, the near-resonant frequency responses of the blade's tip are synthesised based on the extracted modal parameters in Step 5. These synthesised responses are compared to the directly measured ones to validate the extracted modal parameters.

For the fan blade case, the changes in the fundamental harmonic shape of the NNMs are found to be trivial, such that Eq. (22) is solved to synthesise the forced responses. To allow a fine amplitude resolution, Gaussian Process Regression (GPR) models [52] are fitted to the measured discrete points of NNM backbone curves, as shown in Figure 9 and Figure 10. Figure 15 shows the fitting results, where good agreements are observed for the nonlinear modal frequencies and damping ratios. It is also worth mentioning that two subsets of data for NNM 5, separated by a breakpoint, are used to train a piecewise GPR model since one continuous model for this mode always suffers from ill-conditioning.

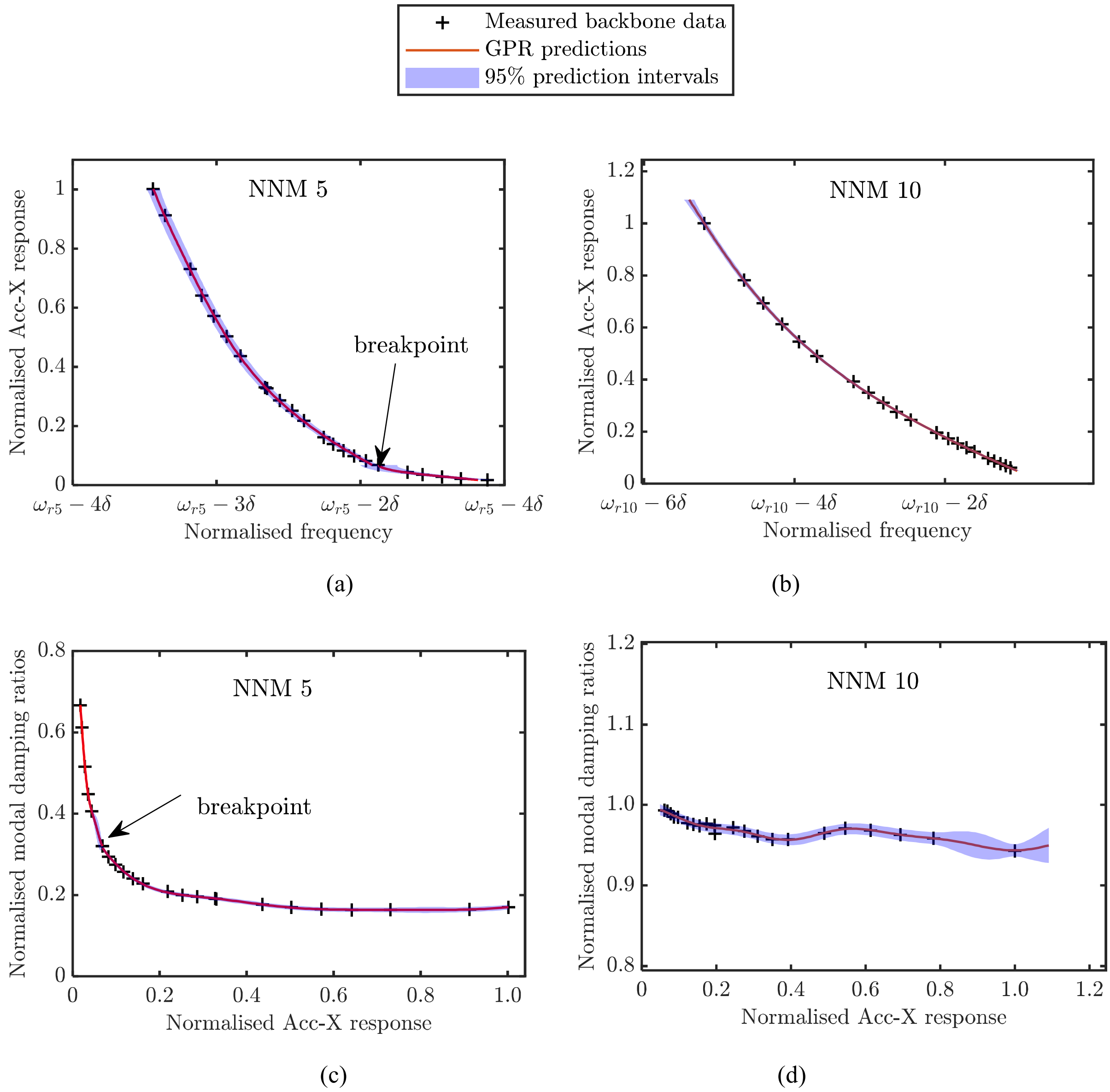


Figure 15. Gaussian Process Regression models of the measured backbone curves: (a) and (b) are modal frequencies of NNM 5 and NNM 10, respectively; (c) and (d) are damping ratios of NNM 5 and NNM 10, respectively.

The near-resonant frequency responses were directly measured using six levels of backward sine-sweeps with a speed of -0.2 Hz/s. For each input level, Eq. (22) is explicitly solved [43,44] using the interpolated values $\tilde{\zeta}_r\left(q_r\right)$ and $\tilde{\omega}_r\left(q_r\right)$ of GPR modes. The predicted forced responses (denoted using '-p') and the measured results (denoted by '-m') are compared in Figure 16.

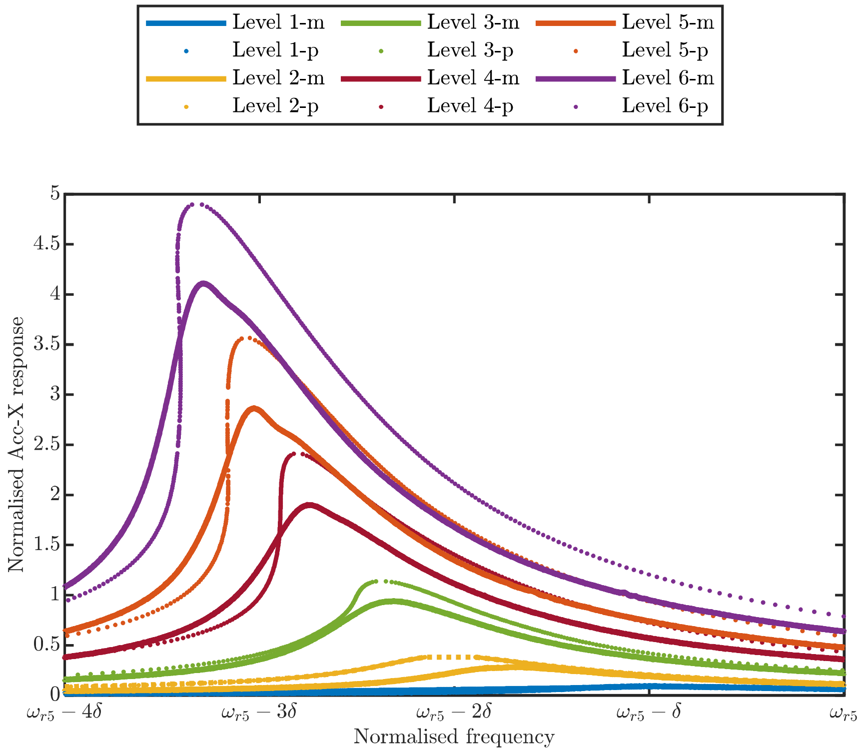


(a)

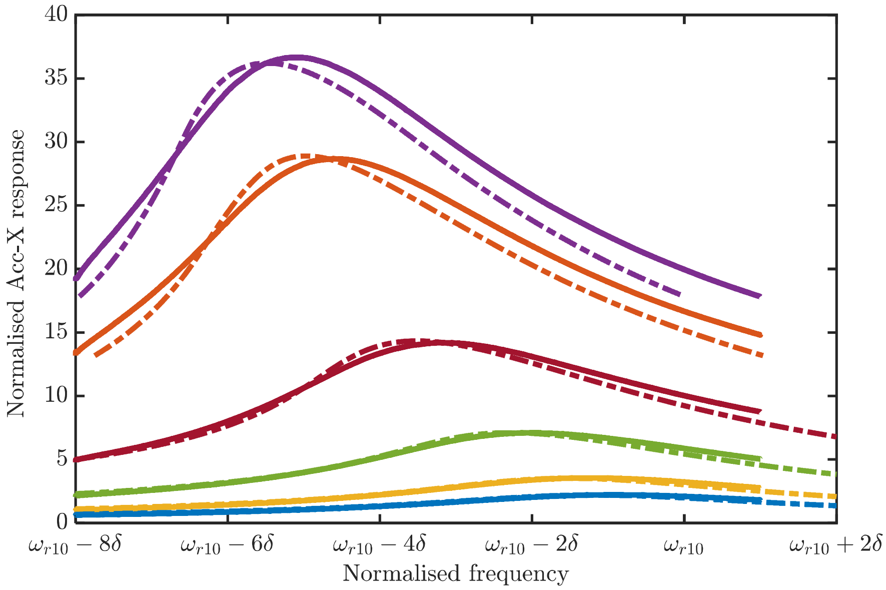


(b)

Figure 16. A comparison of near-resonant frequency responses around (a) NNM 5 and (b) NNM 10: the solid lines are directly measured data, and the dots represent synthesised FRF using the NNM GPR models and nominal input forces.

Surprisingly, as shown in Figure 16 (a), the frequency responses around NNM 5 have substantial discrepancies between the synthesised curves and the directly measured ones. As much as 25% differences in peak amplitudes are observed despite the overall softening trend being captured well. On the other hand, Figure 16 (b) shows the frequency responses around NNM 10, and reasonably good agreements are achieved for this mode. The reason for these discrepancies is found to be the well-known 'force-drop' phenomenon when measuring frequency responses, in which the input force fluctuates around the 'nominal' levels during sine-sweeps. Figure 17 shows a zoom-in view of the actual measured input forces for NNM 5 and NNM 10, respectively. It is shown that a substantial amount of force drops occur for NNM 5 and result in large errors when using the nominal forcing level to predict the forced responses.

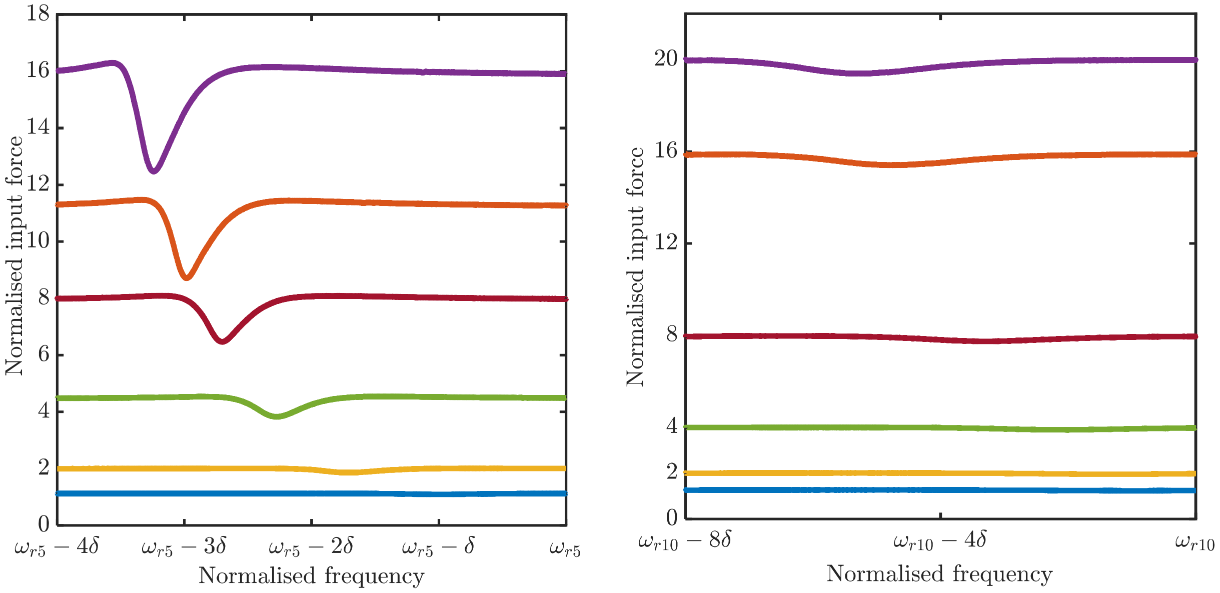


(a) (b)

Figure 17. Zoom-in view of the measured input forces during sine-sweeps for (a) NNM 5 and (b) NNM 10.

To address this issue for NNM 5, a modified synthesis of frequency response curves (denoted using '-mp') using the actual measured input forces (shown in Figure 17) is conducted. Figure 18 compares the modified synthesised results to the directly measured counterparts around NNM 5. It is shown that the modified synthesised curves achieve a much better agreement with the directly measured ones. An additional peak on the left side of the response curves appears in the synthesised curve, which may be attributed to the transient dynamics in the swept-sine testing since backward sweeps are used. Overall, the modified synthesised responses reach satisfactory accuracy for multiple input levels, indicating that the extracted nonlinear modal parameters are of good quality.

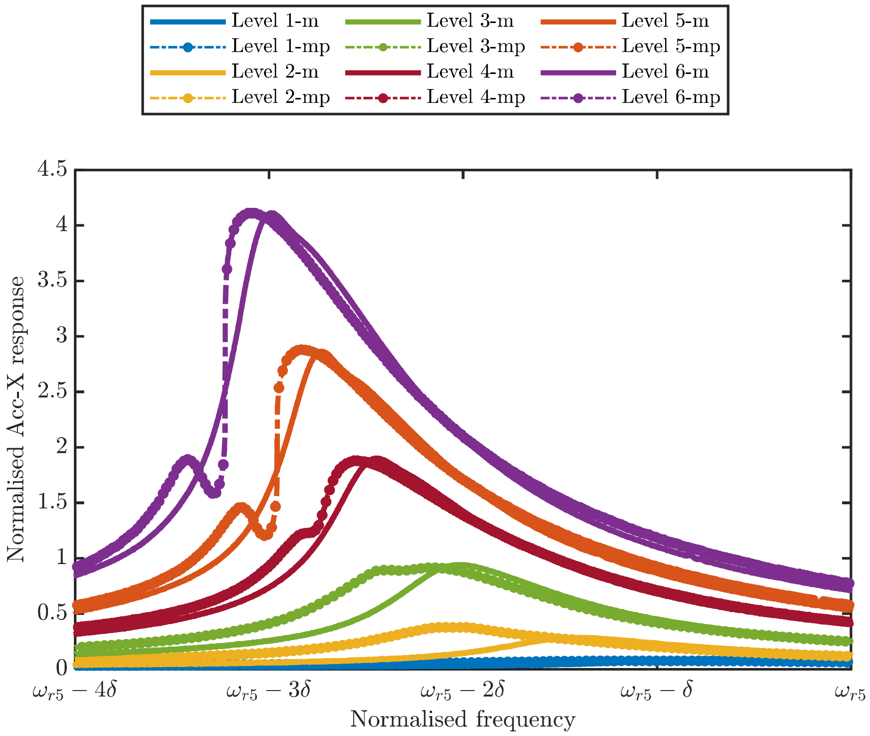


Figure 18. A comparison of near-resonant frequency responses around NNM 5, where solid lines are directly measured data, and dotted lines represent modified synthesised curves using measured input forces.

### C. Phase III: Final Check

At the end of the test campaign, it is crucial to verify that the test structure has not been over-tested or damaged during the high-amplitude nonlinear modal testing. The fan blade was subjected to a low-amplitude excitation, which was the same as that used in Step 1 of Phase Ⅰ. The measured FRFs are compared in Figure 19. The excellent agreement indicates that there were no damage or recognisable structural changes during the test campaign.

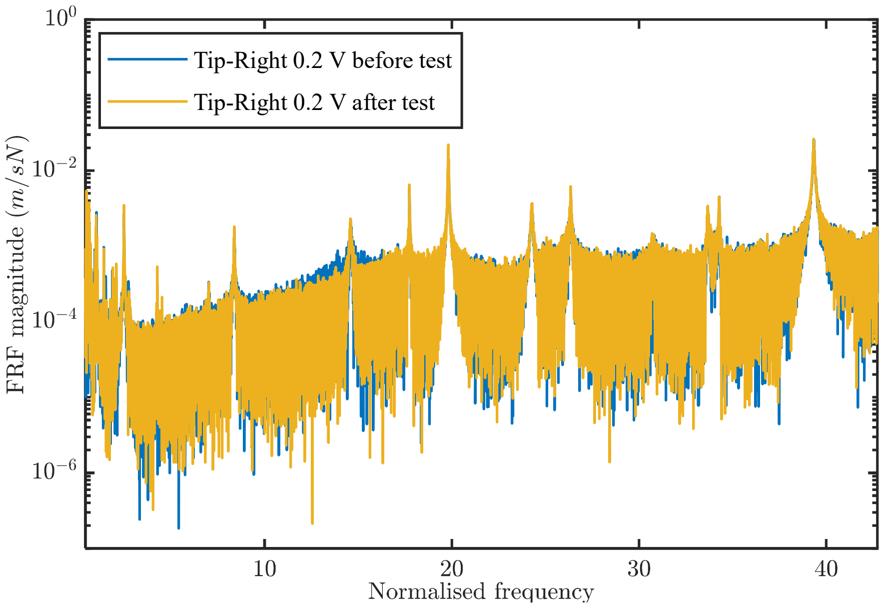


Figure 19. A comparison of y-directional FRFs of the TipRight point before and after the test campaign.

## V. Conclusions

This paper presents a full-field measurement strategy for lightweight nonlinear structures using 3D SLDV. The test setup uses a non-contact 3D SLDV in combination with a MISO vibration controller to measure NNM parameters. The proposed test strategy comprises three major phases. In Phase I, conventional full-field modal testing is conducted to measure the underlying linear modal parameters of the test structure, allowing the nonlinear modal parameters to be linked to these underlying linear modal parameters using a set of non-dimensional numbers. It offers a convenient way to estimate nonlinear damping ratios with minimal manipulation of experimental data. Phase II detects NNMs and quantifies their backbone curves using fast phase-resonance testing, in which sinusoidal excitations were used to measure the amplitude-dependent natural frequencies and modal damping ratios. Note that even when small amplitudes of excitations were used, the measured results may differ from the underlying linear values estimated in Phase I. Thereafter, the highly detailed, multi-harmonic mode shapes are quantified using sine-dwell testing along each backbone curve. In this step, it is necessary to monitor the phase resonance condition for each scan point and apply strict requirements of the phase lag criterion to identify and reject any outliers among the scan points. Phase II ends with a validation of the extracted NNM parameter by synthesising frequency responses and comparing them to the directly measured ones. Particular attention should be paid to the directly measured ones since force drops may occur during the frequency sweeps and result in discrepancies between the synthesised and measured values. Finally, in Phase III, a check of the structural integrity is performed.

The test setup and proposed strategy are demonstrated on a realistic, full-scale fan blade featuring complex geometry and softening nonlinear behaviours. Resulting have shown that all three modal parameters - nonlinear modal frequency, nonlinear damping ratio and full-field multi-harmonic mode shape of the two NNMs are quantified with fine frequency and spatial resolutions that meet stringent industry standards. The critical steps for making this strategy time-efficient while maintaining the frequency resolution and data accuracy are twofold: 1) a proper combination of phase separation and phase resonance techniques; 2) the use of super-short time intervals for each scan point in a full-field test setting. Unique advantages of the proposed measurement strategy include a high sampling rate (12.5 kHz used in this paper), a fine displacement resolution, and a fine frequency resolution, making it suitable for the full-field measurement of industrial-scale structures.

## Acknowledgement

The authors express their gratitude to Rolls-Royce plc and EPSRC for the support under the Prosperity Partnership Grant\Cornerstone: Mechanical Engineering Science to Enable Aero Propulsion Futures, Grant Ref: EP/R004951/1. This research is also funded by the Shenzhen Science and Technology Program (Grants No. RCYX20210706092137055, ZDSYS20210623091808026 and No. 202206193000001, 20220815155101002). Additionally, X.W. would like to thank the National Natural Science Foundation of China under Grants 52005522 and 12072378 for providing financial support. J.Y. acknowledges the funding support from the research grant from the Royal Society of Edinburgh (RSE/1754 and RSE/1865).

## References

[1] Setio, S., H. D. Setio, and L. Jezequel. "A method of non-linear modal identification from frequency response tests." *Journal of Sound and Vibration*, Vol. 158, No. 3, 1992, pp. 497-515.
https://doi.org/10.1016/0022-460X(92)90421-S

[2] Gibert, C. "Fitting measured frequency response using non-linear modes." *Mechanical systems and signal processing*, Vol. 17, No. 1, 2003, pp. 211-218.
https://doi.org/10.1006/mssp.2002.1562

[3] Wang, X., and G. T. Zheng. "Equivalent Dynamic Stiffness Mapping technique for identifying nonlinear structural elements from frequency response functions. " *Mechanical Systems and Signal Processing*, Vol. 68, 2016, pp. 394-415.
https://doi.org/10.1016/j.ymssp.2015.07.011

[4] Wang, Xing, Thomas L. Hill, and Simon A. Neild. "Frequency response expansion strategy for nonlinear structures." *Mechanical Systems and Signal Processing*, Vol. 116, 2019, pp. 505-529.
https://doi.org/10.1016/j.ymssp.2018.06.027

[5] Arslan, Ö., and Özgüven, H. N. "Modal identification of non-linear structures and the use of modal model in structural dynamic analysis. " *Proceedings of the 26th International Modal Analysis Conference (IMAC)*, Orlando, USA, 2008.

[6] Karaağaçlı, T., and Özgüven, H. N. "Experimental modal analysis of nonlinear systems by using response-controlled stepped-sine testing. " *Mechanical Systems and Signal Processing*, Vol. 146, 2021, p. 107023.
https://doi.org/10.1016/j.ymssp.2020.107023

[7] Zhang, Genbei, Chaoping Zang, and Michael I. Friswell. "Measurement of the multivalued phase curves of a strongly nonlinear system by fixed frequency tests. " *Archive of Applied Mechanics*, Vol. 90, 2020, pp. 2543-2560.
https://doi.org/10.1007/s00419-020-01736-w

[8] Platten, M. F., Wright, J. R., Dimitriadis, G., and Cooper, J. E. "Identification of multi-degree of freedom non-linear systems using an extended modal space model. " *Mechanical Systems and Signal Processing*, Vol. 23, No. 1, 2009, pp. 8-29.

https://doi.org/10.1016/j.ymssp.2007.11.016

[9] Peeters, Maxime, Gaëtan Kerschen, and Jean-Claude Golinval. "Dynamic testing of nonlinear vibrating structures using nonlinear normal modes." *Journal of Sound and Vibration*, Vol. 330, No. 3, 2011, pp. 486-509.

https://doi.org/10.1016/j.jsv.2010.08.028

[10] Peeters, Maxime, Gaëtan Kerschen, and Jean-Claude Golinval. "Modal testing of nonlinear vibrating structures based on nonlinear normal modes: Experimental demonstration." *Mechanical Systems and Signal Processing*, Vol. 25, No.4, 2011, pp. 1227-1247.

https://doi.org/10.1016/j.ymssp.2010.11.006

[11] Peter, S., and Remco I. L. "Excitation power quantities in phase resonance testing of nonlinear systems with phase-locked-loop excitation." *Mechanical Systems and Signal Processing*, Vol. 96, 2017, pp. 139-158.

https://doi.org/10.1016/j.ymssp.2017.04.011

[12] Scheel, M., Peter, S., Leine, R. I., and Krack, M. "A phase resonance approach for modal testing of structures with nonlinear dissipation. " *Journal of Sound and Vibration*, Vol. 435, 2018, pp. 56-73.

https://doi.org/10.1016/j.jsv.2018.07.010

[13]Schwarz, S., Kohlmann, L., Hartung, A., Gross, J., Scheel, M., and Krack, M. "Validation of a turbine blade component test with frictional contacts by phase-locked-loop and force-controlled measurements. " *Journal of Engineering for Gas Turbines and Power* , Vol. 142, No. 5, 2020, p. 051006.

https://doi.org/10.1115/1.4044772

[14] Sieber, J., and Bernd, K. "Control based bifurcation analysis for experiments". *Nonlinear Dynamics*, Vol. 51, No. 3, 2008, pp. 365-377.

https://doi.org/10.1007/s11071-007-9217-2

[15] Barton, DAW., Brian P. Mann, and Stephen G. Burrow. "Control-based continuation for investigating nonlinear experiments. " *Journal of Vibration and Control*, Vol. 18, No. 4, 2012, pp. 509-520.
https://doi.org/10.1177/1077546310384004

[16] Renson, L., Gonzalez-Buelga, A., Barton, D. A. W., and Neild, S. A. "Robust identification of backbone curves using control-based continuation. " *Journal of Sound and Vibration*, Vol. 367, 2016, pp. 145-158.
https://doi.org/10.1016/j.jsv.2015.12.035

[17] Beregi, S., Barton, D. A., Rezgui, D., and Neild, S. A. "Robustness of nonlinear parameter identification in the presence of process noise using control-based continuation. " *Nonlinear Dynamics*, 2021, pp.1-16.
https://doi.org/10.1007/s11071-021-06347-w

[18] Wang, X., Szydlowski, M., Yuan, J., and Schwingshackl, C. "An interpolated FFT algorithm for full-field nonlinear modal testing with a 3D-SLDV. " *International Conference on Noise and Vibration Engineering*, Katholieke Universiteit Leuven, 2020, pp. 2261-2274.

[19] Wang, X., Szydlowski, M., Yuan, J., and Schwingshackl, C. "A Multi-step Interpolated-FFT procedure for full-field nonlinear modal testing of turbomachinery components. " *Mechanical Systems and Signal Processing*, Vol. 169, 2022, p. 108771.
https://doi.org/10.1016/j.ymssp.2021.108771

[20] Abeloos, G., Müller, F., Ferhatoglu, E., Scheel, M., Collette, C., Kerschen, G., Brake, M.R.W., Tiso, P., Renson, L., Krack, M. "A consistency analysis of phase-locked-loop testing and control-based continuation for a geometrically nonlinear frictional system." *Mechanical Systems and Signal Processing*, Vol. 170, 2022, p. 108820.
https://doi.org/10.1016/j.ymssp.2022.108820

[21] Farokhi, Hamed, Yiwei Xia, and Alper Erturk. "Experimentally validated geometrically exact model for extreme nonlinear motions of cantilevers." *Nonlinear dynamics* , Vol. 107, 2022, pp. 457-475.

https://doi.org/10.1007/s11071-021-07023-9

[22] Chen, W., Jana, D., Singh, A., Jin, M., Cenedese, M., Kosova, G., Brake, M.R.W., Schwingshackl, C.W., Nagarajaiah, S., Moore, K.J., Noël, J.P. "Measurement and identification of the nonlinear dynamics of a jointed structure using full-field data, Part I: Measurement of nonlinear dynamics. " *Mechanical Systems and Signal Processing*, Vol. 166, 2022, p. 108401.

https://doi.org/10.1016/j.ymssp.2021.108401

[23] Rothberg, S.J., Allen, M.S., Castellini, P., Di Maio, D., Dirckx, J.J.J., Ewins, D.J., Halkon, B.J., Muyshondt, P., Paone, N., Ryan, T., Steger, H., Tomasini, E.P., Vanlanduit, S., Vignola, J.F. "An international review of laser Doppler vibrometry: Making light work of vibration measurement. " *Optics and Lasers in Engineering*, Vol. 99, 2017, pp. 11-22.

https://doi.org/10.1016/j.optlaseng.2016.10.023

[24] Balasubramanian, P., Ferrari G., and Amabili, M. "Identification of the viscoelastic response and nonlinear damping of a rubber plate in nonlinear vibration regime. " *Mechanical Systems and Signal Processing*, Vol. 111, 2018, pp. 376-398.

https://doi.org/10.1016/j.ymssp.2018.03.061

[25] Colin, M., Thomas, O., Grondel, S., and Cattan, É. "Very large amplitude vibrations of flexible structures: Experimental identification and validation of a quadratic drag damping model." *Journal of Fluids and Structures*, Vol. 97, 2020, p. 103056.

https://doi.org/10.1016/j.jfluidstructs.2020.103056

[26] Di Maio, D., Castellini. P., Martarelli, M., Rothberg, S., Allen, M.S., Zhu, W.D., Ewins, D.J. "Continuous Scanning Laser Vibrometry: A raison d'être and applications to vibration measurements." *Mechanical systems and signal processing*, Vol. 156, 2021, p. 107573.

https://doi.org/10.1016/j.ymssp.2020.107573

[27] Ehrhardt, D.A., Allen, M.S., Yang, S., and Beberniss, T.J. "Full-field linear and nonlinear measurements using continuous-scan laser doppler vibrometry and high speed three-dimensional digital image correlation." *Mechanical Systems and Signal Processing*, Vol. 86, 2017, pp. 82-97.

https://doi.org/10.1016/j.ymssp.2015.12.003

[28] Ehrhardt, D.A., Allen, M.S., Beberniss, T.J., and Neild, S.A. "Finite element model calibration of a nonlinear perforated plate." *Journal of Sound and Vibration*, Vol. 392, 2017, pp. 280-294.

https://doi.org/10.1016/j.jsv.2016.12.037

[29] Sever, I. A., and Maguire, M. "Correlation of Full-Field Dynamic Strain Measurements with Reverse Engineered Finite Element Model Predictions." *Experimental Techniques*, Vol. **45,** 2021, pp. 377-387.

https://doi.org/10.1007/s40799-020-00410-8

[30] Kerschen, G., Peeters, M., Golinval, J.C., Vakakis, A.F. "Nonlinear normal modes, Part I: A useful framework for the structural dynamicist." *Mechanical Systems and Signal Processing*, Vol. 23, No. 1, 2009, pp. 170-194.

https://doi.org/10.1016/j.ymssp.2008.04.002

[ 31 ] Krack, M. "Nonlinear modal analysis of nonconservative systems: extension of the periodic motion concept." *Computers & Structures*, Vol. 154, 2015, pp. 59-71.

https://doi.org/10.1016/j.compstruc.2015.03.008

[ 32 ] Renson, L., Kerschen, G., Cochelin, B. "Numerical computation of nonlinear normal modes in mechanical engineering. " *Journal of Sound and Vibration*, Vol. 364, 2016, pp. 177-206.

https://doi.org/10.1016/j.jsv.2015.09.033

[33] Szemplinska-Stupnicka, W. "Non-linear normal modes and the generalized Ritz method in the problems of vibrations of non-linear elastic continuous systems." *International journal of Non-linear Mechanics*, Vol. 18, No. 2, 1983, pp. 149-165.

https://doi.org/10.1016/0020-7462(83)90042-2

[34] Krack, M., Panning-von S.L., and Wallaschek, J. "A method for nonlinear modal analysis and synthesis: Application to harmonically forced and self-excited mechanical systems. " *Journal of Sound and Vibration*, Vol. 332, No. 25, 2013, pp. 6798-6814.

https://doi.org/10.1016/j.jsv.2013.08.009

[35] Peter, S., Scheel, M., Krack, M., and Leine, R.I. "Synthesis of nonlinear frequency responses with experimentally extracted nonlinear modes." *Mechanical Systems and Signal Processing*, Vol. 101, 2018, pp. 498-515.

https://doi.org/10.1016/j.ymssp.2017.09.014

[36] Wright, J.R., Cooper, J.E., and Desforges, M.J. "Normal-mode force appropriation-theory and application. " *Mechanical Systems and Signal Processing*, Vol. 13, No. 2, 1999, pp. 217-240.

https://doi.org/10.1006/mssp.1998.1214

[37] Breunung, T., and Haller, H. "Explicit backbone curves from spectral submanifolds of forced-damped nonlinear mechanical systems." *Proceedings of the Royal Society A: Mathematical, Physical and Engineering Sciences*, Vol. 474, No. 2213, 2018, p. 20180083.

https://doi.org/10.1098/rspa.2018.0083

[38] Nayfeh A.H., and Mook D.T. "Nonlinear oscillations", *John Wiley and Sons, Hoboken*, 1995.

http://dx.doi.org/10.1002/9783527617586

[39] Klotter, K. "Steady state vibrations in systems having arbitrary restoring and arbitrary damping forces." *Proceedings of the Symposium on Nonlinear Circuit Analysis.* Polytechnic Institute of Brooklyn, 1953, Vol. 2, p. 234.

[40] Ewins, D.J. " Modal Testing: Theory, Practice and Application." *John Wiley & Sons*, 2009.

[41] Roettgen, D.R., and Allen, M.S. "Nonlinear characterization of a bolted, industrial structure using a modal framework." *Mechanical systems and signal processing*, Vol. 84, 2017, pp. 152-170.

https://doi.org/10.1016/j.ymssp.2015.11.010

[42] Richardson, M.H. "Is it a mode shape, or an operating deflection shape? " *Sound and Vibration*, March 1997.

[43] Scheel, M. "Nonlinear modal testing of damped structures: Velocity feedback vs. phase resonance." *Mechanical Systems and Signal Processing*, Vol. 165, 2022, p. 108305.
https://doi.org/10.1016/j.ymssp.2021.108305

[44] Wang, X., Guan, X., and Zheng, G. "Inverse solution technique of steady-state responses for local nonlinear structures." *Mechanical Systems and Signal Processing*, Vol. 70, 2016, pp. 1085-1096.
https://doi.org/10.1016/j.ymssp.2015.07.026

[45] Ewins, D.J., Weekes, B., and Delli Carri, A. "Modal testing for model validation of structures with discrete nonlinearities." *Philosophical Transactions of the Royal Society A: Mathematical, Physical and Engineering Sciences*, Vol. 373, 2015, p. 20140410.
https://doi.org/10.1098/rsta.2014.0410

[46] https://www.polytec.com/eu/vibrometry/products/full-field-vibrometers/psv-500-scanning-vibrometer

[47] Kerschen, G., Worden, K., Vakakis, A.F., and Golinval, J.C. "Past, present and future of nonlinear system identification in structural dynamics." *Mechanical systems and signal processing*, Vol. 20, No. 3, 2006, pp. 505-592.
https://doi.org/10.1016/j.ymssp.2005.04.008

[48] Wang, X., Hill, T.L., Neild, S.A., Shaw, A.D., Khodaparast, H.H., and Friswell, M.I. "Model updating strategy for structures with localised nonlinearities using frequency response measurements." *Mechanical Systems and Signal Processing*, Vol. 100, 2018, pp. 940-961.
https://doi.org/10.1016/j.ymssp.2017.08.004

[49] Ozdemir, A.A., and Gumussoy, S. "Transfer Function Estimation in System Identification Toolbox via Vector Fitting." *Proceedings of the 20th World Congress of the International Federation of Automatic Control*, Toulouse, France, July 2017.
https://doi.org/10.1016/j.ifacol.2017.08.1026

[50] Krack, M. "Extension of the single-nonlinear-mode theory by linear attachments and application to exciter-structure interaction." *Journal of Sound and Vibration*, Vol. 505, 2021, p. 116120. https://doi.org/10.1016/j.jsv.2021.116120

[51] Pacini, B.R., Kuether, R.J., and Roettgen, D.R. "Shaker-structure interaction modeling and analysis for nonlinear force appropriation testing." *Mechanical Systems and Signal Processing*, Vol. 162, 2022, p. 108000. https://doi.org/10.1016/j.ymssp.2021.108000

[52] Rasmussen, C.E. and Williams, C.K.I. "Gaussian Processes for Machine Learning." *MIT Press*. Cambridge, Massachusetts, 2006.